Title

cis-B7:CD28 interactions at invaginated synaptic membranes provide CD28 co-stimulation and promote CD8+ T cell function and anti-tumor immunity

Permalink

https://escholarship.org/uc/item/9v07s7n1

Journal

Immunity, 56(6)

ISSN

1074-7613

Authors

Zhao, Yunlong

Caron, Christine

Chan, Ya-Yuan

et al.

Publication Date

2023-06-01

DOI

10.1016/j.immuni.2023.04.005

Peer reviewed

HHS Public Access

Cis-B7:CD28 Interactions at Invaginated Synaptic Membranes Activate CD28 and Promote CD8+ T Cell Function and Anti-Tumor Immunity

Yunlong Zhao[1,*], **Christine Caron**[2], **Ya-Yuan Chan**[1], **Calvin K. Lee**[2], **Xiaozheng Xu**[1,4], **Jibin Zhang**[1], **Takeya Masubuchi**[1], **Chuan Wu**[3], **Jack D. Bui**[2,*], **Enfu Hui**[1,5,*]

[1]Department of Cell and Developmental Biology, School of Biological Sciences, University of California San Diego; La Jolla, CA 92093, USA

[2]Department of Pathology, University of California San Diego; La Jolla, CA 92093, USA

[3]Experimental Immunology Branch, National Cancer Institute, NIH, Bethesda, MD 20892 USA

[4]Present address: Sanofi Institute for Biomedical Research;100 Chongwen Rd, Soochow Industrial Park, Jiangsu Province, China, 215123

[5]Lead Contact

Summary

B7 ligands (CD80 and CD86), expressed by professional antigen presenting cells (APCs), activate the main costimulatory receptor CD28 on T cells in *trans*. However, in peripheral tissues, APCs expressing B7 ligands are relatively scarce. This raises the questions of whether and how CD28 costimulation occurs in peripheral tissues. Here, we report that CD8+ T cells displayed B7 ligands that interacted with CD28 in *cis* at membrane invaginations of the immunological synapse, as a result of membrane remodeling driven by phosphoinositide-3-kinase (PI3K) and sorting-nexin-9 (SNX9). *Cis*-B7:CD28 interactions triggered CD28 signaling through protein-kinase-C-theta (PKCθ) and promoted CD8+ T cell survival, migration and cytokine production. In mouse tumor models, loss of T cell-intrinsic *cis*-B7:CD28 interactions decreased intratumoral T cells and

accelerated tumor growth. Thus, B7 ligands on CD8^{+} T cells can evoke cell autonomous CD28 costimulation in *cis* in peripheral tissues, suggesting *cis*-signaling as a general mechanism for boosting T cell functionality.

eTOC blurb:

Classically, B7 ligands on antigen presenting cells (APC) activate the T cell costimulatory receptor, CD28. Zhao et al. reveal that B7 on T cells can activate CD28 in *cis* at endocytosis-associated membrane curvatures. This cis-signaling promotes anti-tumor T cell responses and explains how T cells sustain functionality in APC-sparse tissues.

Introduction

CD28 is a costimulatory receptor expressed on all mouse and human T cells at birth that regulates T-cell-receptor (TCR) responses both quantitatively and qualitatively.[1–4] Aging-associated loss of CD28 in human T cells is correlated with compromised immune responses to pathogens.[5–7] Aberrant CD28 signaling is a defining feature of T cell dysfunction in cancer, autoimmunity and viral infection.[8–10] Although earlier work suggested that CD28 is more important for CD4^{+} T cells, its significance in CD8^{+} T cells is being increasingly recognized, including priming naïve CD8^{+} T cells and regulating effector and memory CD8^{+} T cells.[11–13]

CD28 has two ligands, B7–1 (CD80) and B7–2 (CD86), best known to be expressed on professional antigen presenting cells (APCs).[14] B7:CD28 *trans*-interactions in the secondary lymphoid organs trigger critical signal 2 alongside TCR ligation that promotes T cell proliferation, survival, migration and cytokine production.[3] However, B7 ligands can be limited in peripheral tissues due to the general lack of B7 expression on non-immune cells, raising the questions of whether and how CD28 costimulation might occur in tissues. B7 ligands are also displayed by T cells, either through translation of T-cell-intrinsic CD80 and CD86 mRNAs or trogocytosis, a process by which T cells acquire membrane proteins from APCs upon physical contact.[15–18] In mice with experimental autoimmune encephalomyelitis, T cells are the main B7-expressing cells in pathological tissues[19] However, the physiological significance of T cell B7 is unclear.

Here we hypothesized that CD28 can interact with B7 in *cis* on the T cell surface/ membrane for costimulation. We determined the existence, topological requirement, subcellular localization and physiological consequence of *cis*-B7:CD28 interactions. We provide evidence that *cis*-B7:CD28 signaling occurs at invaginated synaptic membranes and promotes anti-tumor activity of effector CD8^{+} T cells.

Results

A Subpopulation of CD8^{+} T cells Co-express CD28 and B7 ligands

In light of previous reports of B7 expression by T cells,[15,18,20] we used flow cytometry to measure CD80 and CD86 surface expression kinetics on OT-1 transgenic CD8^{+} T cells primed by ovalbumin peptide 257–264 (OVA$_{257-264}$). CD80 and CD86 were expressed

on a subset of naïve OT-1 cells, and elevated upon peptide stimulation. The frequency of CD28^{+}CD80^{+} and CD28^{+}CD86^{+} OT-1 cells reached 82% and 71% respectively (Figure 1A, see Figure S1 for gating strategy). Thus, CD8^{+} T cells co-express CD28 and B7 ligands especially after antigen exposure.

Both CD80 and CD86 Interact with CD28 in *Cis*

To determine whether CD28 associates with B7 in *cis*, as indicated by prior colocalization analyses,[21,22] we used super-resolution stochastic optical reconstruction microscopy (STORM) to examine the sub-diffraction association of CD28 and B7. We co-expressed CD28 with SpyTagged-CD80, CD86, or PDL1 (negative control) in HEK293T cells, stained CD28 with CF568-labeled antibody, and Spy-B7 or Spy-PDL1 with JF646-labeled SpyCatcher.[23] STORM imaging of the plasma membrane showed stronger colocalization of CD28 with B7 than with PDL1 (Figure 1B), suggesting physical proximity of co-expressed CD28 and B7 ligands.

To further examine the *cis*-interactions between CD28 and B7, we determined their molecular proximity at a single cell level using microscopy-based Förster resonance energy transfer (FRET). We co-expressed CLIP-tagged CD28 and SNAP-tagged CD80, CD86 or PDL1 in HEK293T cells, and labeled CD28 with CLIP-Dy547 (energy donor), and CD80, CD86 or PDL1 with SNAP-AF647 (energy acceptor). FRET, manifested by the recovery of donor fluorescence upon acceptor photobleaching, was evident between CD28 and B7, and was lower between CD28 and PDL1. Moreover, CD28:B7 FRET was abrogated by abatacept, an immunoglobulin (Ig) fusion protein of CTLA4 that binds B7 tightly and blocks CD28:B7 interactions (Figure 1C). Thus, CD28 can interact with both CD80 and CD86 in *cis*.

Cis-B7:CD28 Interactions Stimulate T Cell Activity

We next examined whether *cis*-B7:CD28 interactions modulate T cell activity using a reporter Jurkat line expressing NFκB:GFP and AP1:mCherry,[24] enabling us to quantify both NFκB and AP1 activities using flow cytometry. Secretion of IL-2, downstream of NFκB and AP1, was also examined. We generated reporter Jurkat lines and Raji APCs stably expressing CD80, CD86, or neither (Figure S2A), enabling coculture conditions in which the B7 ligand was presented to CD28 in *cis*, in *trans*, or both. To minimize potential *trans*-B7:CD28 interactions between T cells, we cultured Jurkat reporter cells with 100-fold excess of Raji APCs.

Under B7-free conditions, TCR stimulation by superantigen staphylococcal enterotoxin E (SEE) induced appreciable NFκB, AP1, and IL-2 signals compared to the SEE-free condition (Figure 2A); these reflected TCR-mediated responses without CD28 signaling. Expression of either CD80 or CD86 on Raji cells, i.e., providing *trans*-B7 to CD28, increased all three signals (Figure 2A), as expected. Expression of CD80 or CD86 on reporter Jurkat cells, i.e., providing *cis*-B7, at amounts comparable to *trans*-B7 (Figure S2A), further enhanced NFκB, AP1, and IL-2 signals (Figure 2A), despite decreased CD28 expression (Figure S2B). Compared to the *cis*-B7 alone, co-existence of *cis*-B7 and *trans*-B7 decreased all three signals (Figure 2A), suggesting that *trans*- and *cis*-B7 compete for CD28.

The *cis*-B7 effects were mediated by CD28 binding and signaling, since abatacept abrogated these effects (Figure 2A), or by deletion of CD28 from Jurkat cells (Figure S2C). Confocal imaging revealed that 98% of Jurkat cells formed contacts with Raji cells, rather than with another Jurkat cell (Figure S2D), suggesting that *trans*-B7:CD28 interactions between Jurkat reporter cells were rare. Altogether, these data suggest that *cis*-B7:CD28 interactions can robustly activate CD28.

To examine the role of B7 on primary T cells, we isolated T cells from wild-type (WT) or B7-deficient ($CD80^{-/-}CD86^{-/-}$) C57BL/6J mice, and primed them with anti-CD3ε and anti-CD28 to induce B7 expression on the WT T cells. Upon restimulation with $CD80^{-/-}CD86^{-/-}$ splenocytes loaded with anti-CD3ε, B7-deficient T cells had a decreased frequency of IFNγ$^+$ cells than WT T cells (Figure 2B), indicating a requirement of T cell B7 in optimal effector activity. For human T cells, we detected both B7$^+$ and B7$^-$ population upon polyclonal stimulation of peripheral blood mononuclear cells (PBMCs) with Staphylococcal enterotoxin B (SEB). Upon restimulation with SEB-loaded $CD80^{-/-}CD86^{-/-}$ Raji cells, both B7$^+$ and B7$^-$ T cells were TCR-activated, as indicated by CD69 expression (Figure S2E). However, more B7$^+$ human T cells became IFNγ$^+$ than their B7$^-$ counterparts (Figure 2C). Collectively, these data suggest that B7 expression enhances IFNγ production by T cells.

Cis-B7:CD28 Interactions Occur in a Head-to-Head Fashion Promoted by Negative Membrane Curvatures

The results that abatacept, known to block *trans*-B7:CD28 interactions, also inhibited *cis*-B7:CD28 FRET and signaling (Figure 1 and 2) imply that *cis*-B7 and *trans*-B7 bind to the same site on CD28. Supportive to this notion, mutations that disrupt *trans*-B7:CD28 interactions, CD28 MYPPPY→SGGG,[25] CD80 Y65A,[26] and CD86 F56A,[26] each inhibited the *cis*-B7:CD28 FRET (Figure 3A). Moreover, molecular docking showed that both CD80 and CD86 bind CD28 most favorably in an antiparallel, head-to-head fashion (Figure 3B). These data suggest that *cis*-B7:CD28 interactions occur in a head-to-head mode, akin to the well-documented *trans*-B7:CD28 interactions.

A head-to-head *cis*-binding would require bending of the proteins or membrane invagination, the latter of which would cause the intracellular domains (ICDs) of the interacting proteins to be further apart. Thus, we distinguished these two possibilities by probing FRET between B7 ICD and CD28 ICD. When ICD-tagged CD28-CLIP and B7-SNAP were co-expressed in HEK293T cells and labeled with Dy547 (donor) and AF647 (acceptor) respectively, we detected little FRET, similar to negative controls in which B7 was blocked by abatacept or replaced with PDL1 (Figure 3C). By contrast, FRET was evident between the ectodomain (ECD)-tagged CD28 and B7, as in Figure 1C. Thus, when B7 and CD28 interact in *cis*, their ICDs are more distal while the ECDs remain proximal, consistent with head-to-head binding. In contrast, parallel experiments on the *cis*-interacting PDL1:CD80 pair[27–29] detected substantial FRET when both proteins were ICD labeled, consistent with side-by-side *cis*-binding (Figure 3C).

We next sought to verify the results of FRET experiments using bimolecular luminescence complementation (BiLC), which couples molecular proximity with the reconstitution of

a functional luciferase.[27,30] We incorporated large and small halves of nano-luciferase (LgBiT and SmBiT) to co-expressed CD28 and B7, respectively, either to the ECD or ICD. Compared to the abatacept-treated condition, luminescence was detected when LgBiT and SmBiT were coupled to the ECDs of CD28 and B7, but not when coupled to the ICDs (Figure 3D and E). In contrast, both the ECD- and ICD-tagged CD80:PDL1 pair exhibited strong luminescence compared to conditions containing atezolizumab, which blocks CD80:PDL1 interaction.[28] *Trans*-B7:CD28 interactions in this experiment were prevented by a large excess of untransfected cells, with most CD28$^+$B7$^+$ cells seen in isolation (Figure S3A). Indeed, a 1:1 mixture of CD28-transfected culture and B7-transfected culture produced little luminescence (Figure 3F). CD28 and B7 expression were comparable across all conditions (Figure S3B, C). Altogether, these data indicate that *cis*-CD28:B7 interactions occur in a head-to-head fashion, in which their ECDs associate but ICDs are apart.

To further test if membrane curvatures regulate *cis*-B7:CD28 interactions, we asked whether inducing artificial negative curvatures promotes *cis*-B7:CD28 interactions. We transfected HEK293T cells with SNAP-B7, CLIP-CD28 or CLIP-PDL1, and curvature inducers (FRB fused to the F-BAR domain of formin-binding-protein-17 [FRB-FBP17], and FKBP fused to a plasma-membrane-targeting sequence CAAX [FKBP-CAAX]). Upon rapamycin (rapa) addition, FKBP recruited F-BAR to the plasma membrane, leading to F-BAR-induced membrane invaginations[31] that strongly enriched FRB-FBP17 due to the matching curvature of the F-BAR domain (Figure 3G, left). In ECD-tagged FRET assays, rapamycin enhanced *cis*-B7:CD28 interactions but not *cis*-CD80:PDL1 interactions in an abatacept sensitive fashion (Figure 3G, right). Thus, negative membrane curvatures promote *cis*-B7:CD28 interactions.

Cis-B7:CD28 Interactions Are Promoted by Endocytosis Associated Membrane Curvatures

Although artificially induced membrane invaginations promoted *cis*-B7:CD28 interactions, we noted considerable *cis*-B7:CD28 interactions in the absence of rapa (Figure 3G), indicating that natural cellular processes can produce negative curvatures required for *cis*-B7:CD28 interactions. Given the association of endocytosis with membrane invagination, we next asked whether endocytosis promotes *cis*-B7:CD28 interactions. Because CD28 is internalized via clathrin-mediated endocytosis (CME),[32] we elected to use a dominant-negative mutant of Eps15 (Eps15DN) that blocks the initiation of CME.[33] Confocal imaging showed that Eps15DN expression in HEK293T cells decreased intracellular CD28 (Figure 4A), consistent with a prior report that CD28 is internalized via CME.[32] When introduced into HEK293T cells, Eps15DN suppressed both SNAP-CD80:CLIP-CD28 FRET and SNAP-CD86:CLIP-CD28 FRET (Figure 4A, B). In contrast, Eps15DN did not affect *cis*-PDL1:CD80 interactions, even though it appeared to inhibit PDL1 internalization (Figure S4A). Thus, endocytosis-associated membrane curvatures promote *cis*-CD28:B7 interactions.

To more specifically test the impact of CD28 endocytosis on *cis*-activation by B7, we examined two CD28 mutants: CD28(Y191F), with impaired endocytosis due to defective phosphoinositide 3-kinase (PI3K) binding;[34] and CD28(CD45TM), with the transmembrane

domain (TMD) replaced by the shorter domain of CD45 to enhance endocytosis as short TMDs typically correlate with endomembrane localizations.[35,36] Indeed, after the surface-exposed population of the foregoing CD28 mutants were stained on ice (an endocytosis-inhibited condition), CD28(Y191F) and CD28(CD45TM) showed impaired and enhanced endocytosis at 37 °C respectively, compared to CD28(WT), evident from both flow cytometry and confocal imaging (Figure 4C).

We next examined how endocytosis mutants affect *cis*-B7:CD28 interactions. We co-transduced SNAP-CD80 or SNAP-CD86 with CLIP-tagged CD28 WT, CD28(Y191F), or CD28(CD45TM) to Jurkat cells, and examined *cis*-B7:CD28 FRET. Compared to CD28(WT), CD28(Y191F) decreased the FRET, while CD28(CD45TM) increased the FRET (Figure 4D). IL-2 secretion downstream of *cis*-signaling showed a similar trend in response to the endocytic abilities of CD28 (Figure 4E), even though CD28 surface expression showed an opposite trend (Figure S4B). In contrast, activation of CD28 by *trans*-B7 did not correlate with endocytic activity: CD28(Y191F) Jurkat cell secreted similar amounts of IL-2 as CD28(WT) (Figure 4F), as reported,[37,38] whereas CD28(CD45TM) Jurkat cell secreted less IL-2 (Figure 4F), likely due to its lower surface expression (Figure S4B). These results suggest that CD28 endocytosis promotes *cis*-B7:CD28 signaling while limiting *trans*-B7:CD28 signaling.

We next combined split-APEX2[39] and transmission electron microscopy (TEM) to probe the curvature preference of *cis*-B7:CD28 complexes. Since direct fusion of CD28 or B7 with split APEX2 extensively localized the fusion protein to the endoplasmic reticulum, we used the SpyTag:SpyCatcher and ALFA-tag:ALFA-nanobody (NbALFA) system[40] to couple split APEX2 to B7 and CD28. We co-expressed Spy-CD80 or Spy-CD86 with ALFA-CD28, or Spy-CD80 with ALFA-PDL1 in Jurkat cells. We then labeled Spy-B7 with SpyCatcher fused to the N-terminal half of APEX2 (AP-SpyCatcher), ALFA-CD28 or ALFA-PDL1 with NbALFA fused to the C-terminal half of APEX2 (EX-NbALFA). Since molecular proximity is a prerequisite for the functional reconstitution of APEX2 from the split partners, we expected to detect APEX2-mediated staining of 3,3'-diaminobenzidine (DAB), a substrate of APEX2, specifically at the sites of *cis*-complexes. In both CD80:CD28 and CD86:CD28 co-expressing cells, TEM revealed dark DAB precipitates at plasma membrane invaginations and vesicles underneath the plasma membrane (Figure 4G). In contrast, in CD80:PDL1 co-expressing cells, DAB precipitates were detected on flat membranes (Figure 4G). These data provided visual evidence that *cis*-B7:CD28 interactions occur at negatively curved membranes.

Cis-B7 Promotes the Accumulation of CD28 and PKCθ at the Immune Synapse and De-sequesters the CD28 Intracellular domain from Membranes

We next investigated the mechanism by which *cis*-B7:CD28 interactions co-stimulate TCR signaling. When *CD28⁺CD80⁻CD86⁻* Jurkat cells contacted SEE-loaded *CD80⁻/⁻CD86⁻/⁻* Raji APCs, CD28 was diffuse along the plasma membrane of Jurkat cell, whereas PKCθ, a common effector for CD28 and TCR,[41–43] was weakly enriched at the Jurkat:Raji cell interface (Figure 5A), likely due to TCR activation. Co-expression of CD80 and CD86 with CD28 on Jurkat cells increased synaptic CD28 and PKCθ, which was abrogated by

abatacept (Figure 5A). Thus, B7:CD28 *cis*-interactions rather than their co-expression per se caused CD28 and PKCθ synaptic recruitment. PKCθ primarily colocalized with CD28 at the synaptic membrane, rather than intracellular vesicles (Figure 5A), suggesting that plasma membrane invaginates rather than vesicles are major sites for *cis*-B7:CD28 signaling. Because *cis*-B7:CD28 interactions occur primarily at invaginated membranes (Figure 4G), the synaptic localization of *cis*-B7:CD28 complexes is consistent with prior reports that the immune synapse (IS) is a focal point of receptor endocytosis.[44,45] Indeed, substitution of CD28(WT) with endocytosis mutant CD28(Y191F) decreased the *cis*-B7-mediated synaptic recruitment of CD28 and PKCθ to similar degrees as CD28(Y209F), wherein the PKCθ docking site was mutated (Figure 5A). The less synaptic localization of CD28(Y209F) compared to CD28(WT) might be due to its inability to recruit Lck,[46] thereby mirroring the CD28(Y191F) phenotype through preventing Y191 phosphorylation. Consistent with this result, both Y191F and Y209F inhibited IL-2 secretion induced by *cis*-B7:CD28 signaling. In contrast, IL-2 induced by *trans*-B7:CD28 signaling was inhibited by Y209F but not by Y191F (Figure 5B). These results suggest that both *trans*- and *cis*-B7:CD28 signaling depend on PKCθ recruitment, but only *cis*-signaling requires PI3K binding.

CD28 signaling is restricted by the association of its basic ICD with acidic membrane lipids, limiting its access to effectors (Figure 5C, top).[47,48] Membrane-sequestration of CD28 ICD can be released by CD80:CD28 interaction.[47] Therefore, we tested whether *cis*-B7 affected the membrane association of CD28 ICD, using a FRET assay as described.[48] In the absence of *cis*-B7, CD28-TFP (donor) and the lipophilic dye Octadecyl Rhodamine B (R18, acceptor) in Jurkat cells exhibited FRET, as evidenced by recovery of TFP fluorescence upon R18 photobleaching (Figure 5C). The presence of *cis*-B7 decreased CD28-TFP:R18 FRET, and this effect was abrogated by abatacept (Figure 5C). Thus, *cis*-B7:CD28 interactions release CD28 ICD from membrane sequestration.

SNX9 Promotes Synaptic Accumulation and Signaling of *Cis*-B7:CD28 Complexes

Since the PI3K-binding deficient mutant CD28(Y191F) cannot be activated by *cis*-B7, we next asked how CD28:PI3K association promotes *cis*-B7:CD28 interactions and its downstream signaling. Upon engagement by *trans*-B7 or agonist antibodies, CD28 recruits a membrane-remodeling protein SNX9, which drives inward membrane tubulation at CD28 microclusters[49] and promotes CD28 endocytosis.[32] Additionally, Y191F mutation inhibits CD28:SNX9 association, indicating that PI3K bridges CD28 and SNX9.[32,49] Based on these studies, we hypothesized that SNX9 regulates *cis*-B7:CD28 interactions through a positive feedback loop involving CD28:PI3K interaction, SNX9 recruitment and SNX9-driven membrane invagination, as depicted in Figure 6A. To test this model, we first determined whether SNX9 deficiency affects B7:CD28 *cis*-FRET in T cells upon their APC contact. We co-expressed CLIP-CD28 and SNAP-CD80 or SNAP-CD86 in either $SNX9^{+/+}CD28^{-/-}$ or $SNX9^{-/-}CD28^{-/-}$ Jurkat cells. Upon conjugation with $CD80^{-/-}CD86^{-/-}$ Raji APCs, $SNX9^{-/-}CD28^{-/-}$ Jurkat cells showed reduced *cis*-B7:CD28 FRET compared to $SNX9^{+/+}CD28^{-/-}$ Jurkat cells (Figure 6B). This suggests that SNX9 promotes *cis*-B7:CD28 interactions. Consistent with the FRET data, SNX9 deficiency decreased *cis*-B7 induced PKCθ recruitment and IL-2 production in CD28-expressing Jurkat cells (Figure 6C, D).

We further examined CD28 and SNX9 colocalization at the IS using Z-stack imaging. We stimulated *CD28(WT)+CD80+CD86+mGFP-SNX9+* or *CD28(Y191F)+CD80+CD86+mGFP-SNX9+* Jurkat cells using a supported lipid bilayer (SLB) containing anti-CD3ε and ICAM1, and acquired Z-stack images from the cell-SLB contact zone to ~15 μm into the cell using Airyscan confocal microscopy. CD28(WT) formed microclusters that colocalized with mGFP-SNX9 (Figure 6E). Z-stack reconstruction images in the *X-Z* and *Y-Z* planes revealed SNX9+ structures that emanated from the synapse, extended into the cell interior, and colocalized with membrane lipids (Figure 6E), consistent with inward membrane tubulation as reported.[50] CD28(WT) exhibited a tooth-like pattern enriched at the base of these SNX9+ membrane structures (Figure 6E, upper row). By contrast, CD28(Y191F) formed few microclusters and did not appear to colocalize with SNX9 foci (Figure 6E, bottom row). Thus, CD28:PI3K interaction is required for CD28 to localize to SNX9-driven membrane invaginations, an environment that promotes *cis*-B7:CD28 interactions.

Pharmacological Blockade of *cis*-B7:CD28 Interactions Inhibits CD8+ T cell Function and Anti-Tumor Activity

We next examined the functional relevance of *cis*-B7:CD28 interactions in CD8+ T cells in *vitro*. Using an in *vitro* model consisting of B16OVA (melanoma H-2K^b cell line expressing the ovalbumin model antigen) and OT-1 T cells (which express a TCR recognizing OVA$_{257-264}$ peptide presented by H-2K^b), we assessed the impact of *cis*-B7:CD28 interactions on cytokine production, proliferation, survival, and migration, which are typically promoted by *trans*-B7:CD28 interactions.[4,51–53] We cocultured OVA$_{257-264}$ and IL-2 primed OT-1 cells, expressing both CD80 and CD86 (Figure 1A), with 5-fold excess B16OVA cells or OVA-deficient B16F10 cells in the presence or absence of abatacept. B16F10 and B16OVA lacked B7 expression as reported,[54] even in the presence of IFNγ, which did induce PDL1 expression on these cells (Figure S5). Moreover, the excess tumor cells quickly outgrew OT-1 cells and prevented T:T contact, evident under light microscopy (Figure S6A), presumably limiting B7:CD28 interactions to the *cis* modality. As compared to B16F10, B16OVA stimulated IL-2, IFNγ, and granzyme B (GzmB) production from OT-1 cells, indicating antigen-dependent T cell activation. Disruption of *cis*-B7:CD28 interactions by abatacept inhibited IL-2, IFNγ, GzmB production and OT-1 cell survival (Figure 7A, B).

Because CD28 regulates memory T cell trafficking,[53] we induced central-memory-like T cells via IL-15[55] and examined the effects of abatacept on OT-1 cell migration (Figure 7C). We found that 60% of IL-15-primed OT-1 cell, but not IL-2-primed effector-like OT-1 cell, migrated cross fibronectin (FN)-coated transwells. Abatacept treatment decreased this migration to 40% (Figure 7C). Transwell migration of OT-1 cell was negligible in the absence of FN coating (Figure 7C), indicating that migration was induced by FN interaction with T cell adhesion molecules such as VLA-4.[56] Because integrin LFA-1 also contributes to T cell migration,[57] we next assessed the impact of *cis*-B7:CD28 interactions on LFA-1 activity by imaging actin foci, a marker of LFA-1 activation.[58] When IL-15-treated, LifeAct-mCherry-transduced OT-1 cells contacted a glass plate containing LFA-1 ligand ICAM1, abatacept treatment reduced actin foci formation as revealed by total

internal reflection fluorescence (TIRF) microscopy (Figure 7D). These data suggest that *cis*-B7:CD28 interactions promote T cell migration via stimulating LFA-1 activity.

Despite the aforementioned effects, abatacept did not affect OT-1 cell proliferation, as shown by Ki67 expression (Figure 7E). Thus, *cis*-B7:CD28 interactions promote multiple functionalities of primed CD8$^+$ T cells, but not proliferation.

To assess the impact of *cis*-B7:CD28 interactions on anti-tumor activity in *vivo*, we adoptively transferred peptide-primed OT-1 T cells into B16OVA-bearing *Cd80*$^{-/-}$*Cd86*$^{-/-}$ C57BL/6J mice in the presence of either abatacept or control IgG (Figure 7F schematic). The B7 deficient background of the host ensured exclusive expression of CD80 and CD86 on OT-1 cells, without *trans*-B7 contribution from professional APCs or CD45$^-$ tumor cells (Figure S6B). After transfer of the primed OT-1 cells on day 5, we found that disruption of B7:CD28 interactions by abatacept promoted tumor growth (Figure 7F, p < 0.01). Histological analysis of 21 tumors revealed limited T:T contacts in tumor tissue (Figure S6C), suggesting that T-cell-intrinsic *cis*-B7:CD28 interactions promote the anti-tumor activity of OT-1 cells.

Abatacept treatment decreased the abundance of OT-1 cells in the tumor (Figures 7G, see Figure S7A for gating strategy), but did not decrease the abundance of circulating OT-1 cells (Figure 7G), suggesting a role for *cis*-B7:CD28 interactions in infiltration and/or survival of T cells in tumor tissue. Given that *cis*-B7:CD28 interactions promoted the migration of memory-like T cells in *vitro* (Figure 7C, D), we specifically examined the memory T cells in the blood and tumor. On Day 26–29 after tumor inoculation, 80% of OT-1 cells in the blood and 40% of OT-1 cells in the tumor had a central memory phenotype (Tcm, CD62L^{high}CD44$^+$), unaffected by abatacept treatment (Figure S7B), indicating no effect of *cis*-B7:C28 interaction on Tcm differentiation. In contrast, abatacept decreased the abundance of tumor-infiltrating Tcm but not circulating Tcm (Figure 7H) and suppressed the effector function of tumor-infiltrating OT-1 cells, decreasing TNFα and IFNγ expression while increasing PD1 expression (Figure 7I, Figure S7C).

A CD28 Mutation that Disrupts *Cis*- but not *Trans*-B7:CD28 Signaling Impairs Anti-Tumor CD8+ T Cell Activity

We next determined the physiological significance of *cis*-B7:CD28 signaling in the presence of *trans*-B7:CD28 signaling. We examined in WT host mice whether the PI3K-binding mutant of CD28, which can undergo *trans*- but not *cis*-signaling (Figure 4E, F), compromises the anti-tumor activity of T cells. We isolated naïve CD8$^+$ T cells from *Cd28*$^{-/-}$ OT-1 mice, and transduced the cells with either *Cd28(WT)* or *Cd28(Y170F)*, the latter of which had the PI3K docking site disrupted, equivalent to Y191F in human CD28. After coculture with OVA-loaded B16F10 cells, *Cd28(Y170F)*-reconstituted OT-1 cells produced less IL-2, IFNγ and GzmB than *Cd28(WT)*-reconstituted cells (Figure 7J), and formed fewer actin foci upon contacting ICAM1-containing plate (Figure S7D). When adoptively transferred to B16OVA-bearing WT C57BL/6J mice, *Cd28(Y170F)*$^+$ OT-1 cells were less capable of inhibiting tumor growth than *Cd28(WT)*$^+$ cells (Figure 7K). Although Y170F had limited effect on TNFα and IFNγ expression, it decreased both total and

Tcm population in tumor but not in blood (Figure 7L–N). These data demonstrate that *cis*-B7:CD28 signaling is required for optimal anti-tumor activity of CD8^{+} T cells.

Discussion

In the current paradigm, CD28 is activated in *trans* by B7 ligands expressed on professional APCs in secondary lymphoid organs.[3,4,59] Here, we showed that B7 ligands displayed by primed T cells activated CD28 in *cis* at negative curvatures of the IS, leading to T-cell-autonomous costimulation that enhanced cytokine production, survival, migration, and anti-tumor activity of primed CD8^{+} T cells.

Effector cells typically require less CD28 costimulation than naïve cells, but our results suggest a role of *cis*-B7:CD28 signaling in effector CD8^{+} cells. This is in line with prior findings that blockade of B7:CD28 interactions prevents anti-PDL1 mediated rescue of CD8^{+} exhausted T cells in lymphocytic choriomeningitis virus and tumor models.[13] Although this prior study did not examine the source of B7, the limited B7 expression in non-lymphoid cells supports the concept that *cis*-B7:CD28 signaling contributes to CD8^{+} T cell effector function. Additionally, CD86 expression on T cells is associated with strong immune responses to acute human hepatitis C virus infection.[18] In the case of cancer, B7-expressing DCs can infiltrate tumors, but are unlikely to provide sufficient *trans*-B7 to T cells because DCs represent only 1% of the total immune infiltrates and predominantly localize at T-cell-sparse marginal regions.[60] The ability of T cell B7 to *cis*-activate CD28 suggests that antigen-experienced T cells are able to auto-stimulate in DC-sparse zones.

Despite *cis*-B7:CD28 signaling, T cell control of tumor growth diminished at late timepoints, suggesting that other factors are required in long-lasting tumor immunity. Indeed, if *cis*-signaling initiates from T cell B7 induction and trogocytosis in the lymph nodes, then the natural endocytosis and degradation of B7 would provide a time limit to this *cis*-signaling. Thus, for effective tumor immunity, renewal of B7 on T cells would need to occur via intratumoral APCs providing B7 for trogocytosis, in essence "re-fueling" T cells for extended activity. This could synergize with releasing the brakes via checkpoint blockade. In fact, the presence, quantity, and type of DCs that inhabit tumors could predict prognosis and responsiveness to immune therapy.[60–63]

Our study suggests that *cis* and *trans*-B7 engage competitive binding to CD28, but either is sufficient for triggering CD28-PKCθ signaling at the IS. *Cis*-CD28 signaling appeared to mirror *trans*-CD28 signaling in promoting survival, migration and cytokine release, but did not enhance proliferation of T cells as does *trans*-CD28 signaling. While this may indicate a distinction between *cis*- and *trans*-CD28 signaling, it could also be due to the use of primed T cells in this study, as opposed to naïve T cells used in prior studies on proliferation. Indeed, the proliferation of primed T cells depends mainly on 4–1BB rather than CD28.[64,65]

Trans-B7:CD28 interactions can occur upon T cell contact with DCs or other T cells[66] as observed during T-cell priming in lymph nodes, where many proliferating T cells cluster with fewer DCs.[67] However, primed T cells disperse from the clusters in about 36 h,[67] and such clusters are not observed in tumor tissues.[60,63] Moreover, our analysis of B16OVA

tumors via immunohistochemistry revealed that individual T cells are surrounded by excess tumor cells. Thus, whereas *trans*-B7:CD28 interactions promote T cell priming in lymphoid organs, *cis*-signaling is likely the major mode of CD28 activation in peripheral tissues due to limited APC:T or T:T contacts, especially in APC-sparse tumors.

CD28-crosslinking can induce actin polymerization even without TCR stimulation.[68] In line with this, blockade of *cis*-B7 inhibited actin foci formation in the absence of TCR signal. This indicates a TCR-independent function of CD28 and that *cis*-B7:CD28 interactions can promote T cell migration into peripheral tissues.

Our results suggest that while *cis*-PDL1:CD80 interactions occur in a side-by-side parallel modality, *cis*-B7:CD28 interactions occur in a head-to-head, anti-parallel configuration that are facilitated by membrane invagination. Indeed, *cis*- but not *trans*-B7:CD28 signaling was positively correlated with CD28 endocytosis. Thus, whereas endocytosis down-modulates cell-cell *trans*-signaling by removing receptors from cell surface,[69] endocytosis-associated membrane curvatures might promote cell-autonomous *cis*-signaling. Conversely, a strained *cis*-complex preformed on flat membranes might partition to endocytosis site for free energy minimization, thereby promoting receptor endocytosis. Indeed, expression of *cis*-B7 decreased CD28 surface expression. Thus, *cis*-signaling and endocytosis might be intrinsically coupled.

Prior studies suggest either required or dispensable roles for PI3K in CD28 signaling.[52,70,71] Here we show that PI3K promotes *cis*- but not *trans*-B7:CD28 signaling through inducing membrane invaginations. Additionally, PI3K might recruit CD28 to pre-existing SNX9-containing membrane curvatures. This notion is supported by the synaptic SNX9 signal seen in a subset of cells expressing the PI3K binding mutant CD28(Y191F). Such SNX9 signals might be due to TCR signaling, known to activate PI3K.[72] However, the lack of synaptic recruitment of CD28(Y191F) suggests that PI3K is required to bridge CD28 and SNX9. CD86 may also directly signal through PI3K,[73] suggesting that *cis*-B7:CD28 interactions might promote signaling through both CD28 and B7. Other PI3K recruiting receptors, such as ICOS, CD2 and CD226, might engage *cis*-signaling via a similar mechanism involving SNX9 or similar membrane remodeling proteins. Indeed, *cis*-signaling mediated by CD2:CD58 interactions has been reported.[74–76]

The extracellular height of a B7:CD28 complex is ~13 nm,[77] thus, their head-to-head *cis*-binding requires closely apposed membranes. Our data suggest that this configuration could be provided by SNX9 induced narrow membrane tubules, with outer diameters measured at 20–100 nm.[49,78,79] A 20 nm lipid tubule would have an inner diameter of ~12 nm that allows B7 and CD28 to interact across the lumen. Such sharp membrane curvatures might also be facilitated by SNX9 paralogs, actin cytoskeleton and dynamin, a membrane constrictor recruited by SNX9.[80]

The present study supports the notion that local membrane curvatures actively modulate receptor signaling. Membrane protrusions such as microvilli can promote T cell activation by sorting signaling molecules.[81,82] Here we show that the PI3K-SNX9 induced tubular invaginations sort *cis*-B7:CD28 complexes to the IS, where TCR signaling components

are also enriched. The juxtaposition of *cis*-B7:CD28 complexes with the TCR presumably allows for efficient *cis*-costimulation. Such tubular invaginations may be considered as *cis*-synapses that promote cell autonomous signaling. Thus, membrane geometry and dynamics represent an underappreciated dimension of T cell signaling and suggest inroads for manipulating T cell activities.

Limitations of the study:

Some schematics of this study assume that *cis*-B7:CD28 interactions occur in a pseudo-*trans* modality at sharp membrane tubules emanating from the immune synapse, but we have not provided definitive visual evidence due to limited resolution of confocal microscopy. Such evidence would require super-resolution microscopy at 3D resolution. Our experimental tumor model addressed the contribution of *cis*-B7:CD28 signaling only during the effector stage of CD8^{+} T cell activity. This model did not allow for long-term studies of *cis*-B7:CD28 signaling in T cell memory formation or maintenance. It models acute inflammation of cancer in humans but does not resemble indolent cancers that form over years in people. Future studies are needed to address the functional relevance of *cis*-B7:CD28 signaling in other T cell subsets, during other stages of the immune response and in other disease settings. Moreover, while abatacept was used in this study as a B7 blocker, we did not address the potential regulation of *cis*-CD28 signaling by endogenous CTLA4. It is likely that the *cis*-B7:CD28 signaling observed here was already mitigated by CTLA4 action. Thus, we expect a greater effect of abatacept or PI3K-binding mutant had CTLA4 been deleted from our system. Likewise, other negative regulators such as PD1 could also reduce the signals observed here in primary cells and tumor models.

STAR Methods

RESOURCE AVAILABILITY

Lead contact—Further information and requests for resources and reagents should be directed to and will be fulfilled by the lead contact, Enfu Hui (enfuhui@ucsd.edu)

Materials availability—All materials supporting the findings of this study are available from the lead author upon reasonable request.

Data and code availability—All data generated supporting the findings of this study are available in the manuscript. Further information is available from the lead author upon reasonable request. This paper does not report original code.

EXPERIMENTAL MODEL AND SUBJECT DETAILS

Cell Cultures—HEK293T cells (RRID: CVCL_0063), Phoenix-ECO cells (RRID: CVCL_H717) and Platinum E cells (RRID: CVCL_B488) were maintained in DMEM medium (Corning, 10017CV) supplemented with 10% fetal bovine serum (Omega Scientific, FB-02), 100 U/mL of Penicillin (GE Healthcare, SV30010), and 100 mg/mL of Streptomycin (GE Healthcare, SV30010) at 37 °C, 5% CO_2. Jurkat cells (RRID: CVCL_0065) and Raji cells (RRID: CVCL_0511) were maintained in RPMI 1640 medium (corning, 10–041-CM) supplemented with 10% fetal bovine serum (FBS), 100 U/mL of

Penicillin, and 100 mg/mL of Streptomycin) at 37 °C, 5% CO_2. Jurkat and Raji cells were authenticated by ATCC using short tandem repeats (STR) profiling. OT-1 splenocytes were harvested from both male and female C57BL/6-Tg (TcraTcrb) 1100Mjb/J (OT-1) mice (Jackson Laboratory) or $Cd28^{-/-}$ OT-1 mice (home-bred). WT and B7 deficient mouse splenocytes were harvested from WT C57BL/6J mice (Jackson Laboratory) and B6.129S4-Cd80tm1Shr Cd86tm2Shr/J ($Cd80^{-/-}$ $Cd86^{-/-}$) mice (Jackson Laboratory). Human PBMCs were isolated from a healthy donor (35-year-old female). All of the primary T cells were maintained in primary T cell medium (RPMI 1640 supplemented with 10% FBS, 1 mM sodium pyruvate [Corning, 25–000-CI], 50 mM β-mercaptoethanol [Fisher Scientific, ICN19024283], 100 U/mL of Penicillin, and 100 mg/mL of Streptomycin) at 37 °C, 5% CO_2. Mouse melanoma lines B16F10 (ATCC, CRL-6475, RRID: CVCL_0159) and B16OVA (ovalbumin transduced B16F10, provided by Ananda Goldrath at University of California San Diego) were maintained as monolayer cultures in primary T cell medium at 37 °C, 5% CO_2. Tumor cells were harvested with 0.25% trypsin-0.02% EDTA. Trypsin was neutralized with medium containing 10% FBS, washed and suspended in HBSS with calcium and magnesium (Thermo Scientific, 14025134) for injection. Cells were used for injections only if the viability was greater than 90% as determined by Trypan Blue (Sigma, T8154). The lack of mycoplasma in the cell lines was confirmed using PCR Mycoplasma Detection Kit (Applied Biological Materials Inc, G238).

Animals—OT-1, WT C57BL/6J; $Cd80^{-/-}Cd86^{-/-}$ C57BL/6J and $Cd28^{-/-}$ C57BL/6J mice were purchased from the Jackson Laboratory. $Cd28^{-/-}$ C57BL/6J mice were bred with OT-1 mice to generate $Cd28^{-/-}$ OT-1 mice, which was verified by genotyping. All mice were housed under pathogen-free conditions at the University of California San Diego (UCSD) with ad libitum access to food and water. In adoptive transfer procedure, mice were anesthetized intraperitoneally with 100 μL 1x PBS containing 16.7 mg/mL ketamine (Cristália) and 3.3 mg/mL Xylazine (Syntec). All procedures were previously reviewed and approved by the UCSD IACUC under protocol S06201 and S18078.

METHOD DETAILS

Cell Lines—Genotypes of Raji cells and Jurkat cells used in this study are summarized in Table S1. All recombinant DNAs used in this study were listed in Table S2.

For Figure 2 and Figure S2A&B, $NF\kappa B:GFP^+AP1:mCherry^+$ reporter Jurkat cell was generated by retrovirally transducing $NF\kappa B:GFP$ and $AP1:mCherry$ reporter into WT Jurkat cell. Jurkat transductants were then sorted for GFP⁺mCherry⁺ double positive using flow cytometry after stimulation with anti-CD3ε (BioLegend, 317326) and anti-CD28 (Bio X cell, BE0291). The sorted cells were rested in culture medium for 1 week and sorted for a second round of to select GFP⁻mCherry⁻ double negative cells under resting state. To generate $CD80^+$ or $CD86^+$ reporter Jurkat cells, $CD80$ or $CD86$ was lentivirally transduced into $NF\kappa B:GFP^+AP1:mCherry^+$ reporter Jurkat cells. $CD80^{-/-}CD86^{-/-}$, $CD80^{+/+}CD86^{-/-}$, and $CD80^{-/-}CD86^{+/+}$ Raji cells were generated previously.[28]

For Figure S2C and Figure 4, to generate $CD28^{-/-}$ Jurkat line, WT Jurkat cells were electroporated with pX330GFP plasmids coding $CD28$

sgRNAs (5'-GCTTGTAGCGTACGACAATG-3' or 5'-GTCCTTTGTGAAGGGATGCC-3'). Electroporated cells were recovered for 2 days at 37 °C, 5% CO_2, sorted for GFP-positive cells and maintained in culture medium. 1 week later, cells were stained with PE anti-CD28 (BioLegend, 302940) and sorted for CD28−GFP− double negative cells. For Figure S2C, *CD28*−/− Jurkat or WT Jurkat cells were lentivirally transduced with either *CD80-mTFP1* or *CD86-mTFP1*.

For Figure 4C, to generate Jurkat lines expressing CD28 endocytosis variants, *CD28*−/− Jurkat cells were lentivirally transduced with *CD28(WT)*, *CD28(Y191F)*, or *CD28(CD45TM)* with an N-terminal Spy-tag.

For FRET assays in Figure 4D, *CD28*−/− Jurkat cells were lentivirally transduced with *CD28(WT)*, *CD28(Y191F)*, or *CD28(CD45TM)* fused with a N-terminal CLIP tag, and then transduced with *CD80* or *CD86* fused with an N-terminal SNAP-tag.

For Figure 4E, double positive Jurkat cells were generated by lentivirally transducing *CD28*−/− Jurkat cells with *CD80* or *CD86*, followed by transduction with *CD28(WT)*, *CD28(Y191F)*, or *CD28(CD45TM)*. In Figure 4F, *CD28*−/− Jurkat cells were lentivirally transduced with *CD28(WT)*, *CD28(Y191F)*, or *CD28(CD45TM)* before coculture with B7-expressing Raji cells.

For Figure 4G, *CD28*−/− Jurkat cells were lentivirally co-transduced with ALFA-tagged *CD28* and Spy-tagged *CD80* or *CD86* before subjected to split APEX labeling and TEM. In the control condition, *CD28*−/− Jurkat cells were transduced with ALFA-tagged *PDL1* and Spy-tagged *CD80*.

For Figure 5A, *CD28*−/− Jurkat cells were lentivirally transduced with *CD28(WT)*, *CD28(Y191F)*, or *CD28(Y209F)*, and then co-transduced with both *CD80* and *CD86* to generate triple positive Jurkat cells. For Figure 5B, *CD28*−/− Jurkat cells were lentivirally transduced with *CD28(WT), CD28(Y191F)*, or *CD28(Y209F)*. For expressing *cis*-CD80, those Jurkat lines were then co-transduced with CLIP-tagged *CD80* to generate double positive Jurkat cells. For Figure 5C, *CD28*−/− Jurkat cells were lentivirally transduced with *CD28-mTFP1*, and then co-transduced with both *CD80* and *CD86* to generate triple positive Jurkat cells.

For Figure 6, *SNX9* was deleted from WT Jurkat or *CD28*−/− Jurkat line by electroporating each cell line with pX330GFP plasmids coding *SNX9* sgRNAs (5'-AATGAACTGACGGTTAATGA-3' and 5'-GAAACATCAAAGGAGAACGA-3').[49] Electroporated cells were recovered for 2 days at 37 °C, 5% CO_2. Single GFP-positive cells were then sorted by flow cytometry and expanded in culture medium for 4 weeks. SNX9 expression in single-cell derived colonies was then examined using western blot with anti-SNX9 antibody (Proteintech, 15721–1-AP), anti-GAPDH antibody (Proteintech, 10494–1-AP) and CF568-labeled anti-rabbit IgG antibody (Biotium, 20801). To examine *cis*-CD28:B7 FRET in Figure 6B, *CD28* fused with an N-terminal CLIP tag was lentivirally transduced into *CD28*−/− Jurkat cells (*CD28*−/−*SNX9*+/+ Jurkat) or *CD28*−/−*SNX9*−/− Jurkat cells, followed by co-transducing *CD80* and *CD86* fused with an N-terminal SNAP-tag. For Figure 6C and E, *CD28*−/−*SNX9*−/− Jurkat cells were first lentivirally transduced with

CD28(WT) or *CD28(Y191F)*, and then transduced with *mGFP-SNX9*, followed by sorting GFP positive cells using flow cytometry. *CD28(WT)⁺SNX9⁻/⁻* Jurkat cells, *CD28(WT) ⁺mGFP-SNX9⁺* Jurkat cells, or *CD28(Y191F)⁺mGFP-SNX9⁺* Jurkat cells were then co-transduced with *CD80* and *CD86* to enable the examination of *cis*-B7:CD28 signaling. For Figure 6D, WT Jurkat cells and *SNX9⁻/⁻* Jurkat cells were co-transduced with *CD80* and *CD86* for measurement of IL-2 secretion using ELISA.

Recombinant Proteins—SpyCatcher,[23] LgBiT-SpyCatcher, SpyCatcher-AVI, and AP-SpyCatcher were expressed with an N-terminal His$_6$ tag in *Escherichia coli* BL21 (DE3) (NEB, C2527I) using a pET28a vector. All His-tagged proteins were purified using a HisTrap HP column (GE Healthcare, 17524802) and eluted using buffer containing 50 mM HEPES-NaOH, pH 8.0, 150 mM NaCl and 0.5 M imidazole. EX-NbALFA was expressed in *Escherichia coli* BL21(DE3) with a GST tag, a SUMO tag, and a PreScission recognition site (LEVLFQGP) fused in sequence at its N-terminus. GST-SUMO-EX-NbALFA was purified using Glutathione Agarose Beads (MCLAB, GAB-300) and the EX-NbALFA moiety was eluted from the agarose using 20 U/ml 3C protease in 20 mM HEPES-NaOH, pH 7.5, 150 mM NaCl, 5 mM b-mercaptoethanol, 0.1% TWEEN20. All affinity-purified proteins were gel filtered using a Superdex 200 Increase 10/300 GL column (GE Healthcare, 28990944) or Superdex 75 Increase 10/300 GL column (GE Healthcare, 29148721) in HEPES buffered saline (50 mM HEPES-NaOH, pH 7.5, 150 mM, NaCl, 10% glycerol). Gel filtrated SpyCatcher was labeled with Janelia Fluor® 646 (JF646) maleimide (Tocris Bioscience, 6590) following manufacturer's instructions. Free dyes were then removed using Zeba Spin Desalting Columns (Thermo Fisher Scientific, P187769). Gel filtrated SpyCatcher-AVI was biotinylated with a home-made BirA protein,[83] and excess biotin together with BirA were removed by gel filtration using Superdex 75 Increase 10/300 GL. All proteins were quantified by SDS-PAGE and Coomassie blue staining, using bovine serum albumin (BSA, Thermo Scientific, 23209) as a standard.

FRET Assays for *Cis*-interactions—For all FRET assays measuring *cis*-interactions, images were acquired with a Leica SP8 confocal microscope by exciting Dy547 at 561 nm and AF647 at 633 nm. Donor and acceptor images before and after acceptor photobleaching were acquired for FRET analysis using ImageJ. To calculate FRET efficiency N_{FRET}, the increased donor fluorescence intensity after acceptor photobleaching was divided by the square root of the product of donor fluorescence intensity and acceptor fluorescence intensity, which was used to normalize expression levels of donor and acceptor fused proteins, as described.[84] FRET image was generated by AccPbFRET plugin in ImageJ.[85]

For Figure 1C, HEK293T cells were co-transfected with a pHR plasmid encoding human *CD28* fused to an N-terminal CLIP tag (*CLIP-CD28*) and a pHR plasmid encoding human *CD80, CD86 or PDL1* fused to an N-terminal SNAP tag (*SNAP-CD80, SNAP-CD86, or SNAP-PDL1*) using polyethylenimine (Fisher Scientific, NC1014320). For Figure 3A, HEK293T cells were co-transfected with *CLIP-CD28* or *CLIP-CD28(SGGG)* and *SNAP-CD80, SNAP-CD80(Y65A), SNAP-CD86, or SNAP-CD86(F65A)*. 20 h after transfection, cells were trypsinized and seeded on a poly-D-lysine (Sigma-Aldrich, P6407) treated glass bottom 96-well plate (Dot Scientific, MGB096–1-2-LG-L). Cells were then labeled with

CLIP-Surface Dy547 (NEB, S9233S) and SNAP-Surface AF647 (NEB, S9136S) at 37 °C, 5% CO_2 for 30 min. For abatacept treated conditions, 20 μg/mL abatacept was included in the staining solution. Labeled cells were then fixed with 4% paraformaldehyde (PFA, Fisher Scientific, 50980494), washed 3 times with 1x PBS (pH 7.4), and used for FRET assays.

For Figure 3C, to determine ICD FRET, HEK293T cells were co-transfected with a pHR plasmid encoding human *CD28* fused to a C-terminal CLIP-tag (*CD28-CLIP*) and a pHR plasmid encoding *CD80* or *CD86* fused to a C-terminal SNAP-tag (*CD80-SNAP* or *CD86-SNAP*). For controls, HEK293T cells were co-transfected with *PDL1-CLIP* and *CD80-SNAP*. 20 h post transfection, cells were trypsinized and seeded on a poly-D-lysine treated glass-bottom 96-well plate. For abatacept treated conditions, cells were incubated with 20 μg/mL abatacept at 37 °C, 5% CO_2 for 30 min. To stain intracellular CLIP and SNAP tags, cells were fixed with 4% PFA, permeabilized by 0.05% Triton X-100 (Fisher BioReagents, BP151500), and labeled with CLIP-Surface Dy547 (NEB, S9233S) and SNAP-Surface AF647 (NEB, S9136S) at 37 °C, 5% CO_2 for 30 min before subjected to FRET assays.

For Figure 3G, to chemically induce membrane invagination simultaneously in a large cell population, the bicistronic opto-FBAR plasmid[31] was modified by replacing the optically inducible dimerization pair iLID:SspB with the chemically inducible dimerization pair FRB:FKBP. The modified bicistronic plasmid FKBP:FRB-FBAR, upon transfection to the HEK293T cells, drove the expression of both plasma membrane targeted 3xFKBP-TagBFP-CAAX and cytoplasmic mGFP-FRB-FBP17. To verify inducible membrane invagination, *FKBP:FRB-FBAR* transfected HEK293T cells were treated with 100 nM rapamycin (Fisher BioReagents, 501126903) for 5 min and tubular membrane structures, marked by strong mGFP-FRB-FBP17 localization, was visualized using confocal microscopy. For FRET assays, *FKBP:FRB-FBAR* was co-transfected with FRET pairs - *CLIP-CD28:SNAP-CD80*, *CLIP-CD28:SNAP-CD86*, or *CLIP-PDL1:SNAP-CD80* - into HEK293T cells. 20 h post transfection, cells were trypsinized and seeded on a poly-D-lysine-treated glass-bottom 96-well plate, followed by labeling with CLIP-Surface Dy547 (NEB, S9233S) and SNAP-Surface AF647 (NEB, S9136S) at 37 °C, 5% CO_2 for 30 min, with or without 20 μg/mL abatacept in the staining solution. Labeled cells were then treated by 100 nM rapamycin or DMSO alone for 5 min at 37 °C and fixed with 4% PFA. Cells were washed thrice with 1x PBS (pH 7.4) before subjected to FRET assays.

For Figure 4B and Figure S4A, HEK293T cells were transfected with *CLIP-CD28:SNAP-CD80*, *CLIP-CD28:SNAP-CD86*, or *CLIP-PDL1:SNAP-CD80* either alone or in combination with a plasmid encoding mGFP-tagged Eps15DN. 20 h post transfection, cells were trypsinized and seeded on a poly-D-lysine-treated glass-bottom 96-well plate, followed by labeling with CLIP-Surface Dy547 (NEB, S9233S) and SNAP-Surface AF647 (NEB, S9136S) at 37 °C, 5% CO_2 for 30 min. Cells were then fixed with 4% PFA before subjected to FRET assays. For measuring CD28 and PDL1 internalization in Figure 4A and Figure S4A, same procedures were used except that *CLIP-CD28* or *CLIP-PDL1* was transfected either alone or in combination with *mGFP-Eps15DN*.

For Figure 4D, Jurkat cells were co-transduced with indicated CD28 variant fused to an N-terminal CLIP tag and either CD80 or CD86 fused to an N-terminal SNAP tag. Transduced cells were seeded on a poly-D-lysine-treated glass-bottom 96-well plate, followed by labeling with CLIP-Surface Dy547 (NEB, S9233S) and SNAP-Surface AF647 (NEB, S9136S) at 37 °C, 5% CO_2 for 30 min. Labeled cells were fixed with 4% PFA, washed thrice with 1x PBS (pH 7.4) before subjected to FRET assays.

For Figure 6B, *CLIP-CD28* and SNAP-CD80 or *SNAP-CD86* co-transduced *CD28$^{-/-}$SNX9$^{+/+}$*Jurkat cells or *CD28$^{-/-}$SNX9$^{-/-}$*Jurkat cells were labeled with CLIP-Surface Dy547 (NEB, S9233S) and SNAP-Surface AF647 (NEB, S9136S) at 37 °C, 5% CO_2 for 30 min. Labeled cells were then conjugated with SEE-loaded *CD80$^{-/-}$CD86$^{-/-}$* Raji cell for another 30 min, fixed with 4% PFA, washed thrice with 1x PBS (pH 7.4) before imaging. Jurkat:Raji cell conjugates were randomly selected under Leica SP8 confocal microscope and subjected to FRET measurements.

FRET Assays for CD28-ICD:Membrane Interactions—For Figure 5C, *CD28-mTFP1$^+$* Jurkat cells and *CD28-mTFP1$^+$CD80$^+$CD86$^+$* Jurkat cells were conjugated with SEE-loaded *CD80$^{-/-}$CD86$^{-/-}$* Raji cells for 30 min, and fixed with 4% PFA. Fixed cells were then stained by 2 μM Octadecyl Rhodamine B Chloride (R18, Biotium, 60033) on ice for 5 min and used for FRET assays shown in Figure 1C. For the abatacept treated condition, Jurkat cells were pre-incubated with 20 μg/mL abatacept for 1 h before co-pelleted with Raji cells. mTFP1 and R18 were excited by 458 nm laser and 543 nm laser respectively using a Zeiss LSM 880 airyscan confocal microscope. N_{FRET} of mTFP1:R18 was calculated at the IS region, defined as the conjugate area between a Jurkat cell and a Raji cell based on the DIC images and the fluorescence channels.

STORM Assay—For Figure 1B, HEK293T cells were seeded on poly-D-lysine treated coverslips and co-transfected with *CD28* and *CD80*, *CD86*, or *PDL1* fused with an N-terminal SpyTag, using polyethyleneimine. 20 h after transfection, cells were fixed with 4% PFA. CD28 was stained with anti-CD28 antibody (Bio X cell, BE0291) and then with CF568-conjugated anti-mouse IgG antibody (Biotium, 20802). Cells were then incubated with home-made JF646-labeled SpyCatcher protein for staining of Spy-CD80, Spy-CD86, and Spy-PDL1, washed thrice with 1x PBS (pH 7.4), and sealed in Everspark STORM buffer (idylle, Everspark). STORM was performed on a Nikon Eclipse Ti2-E Ti2 inverted microscope equipped with TIRF configuration. The excitation lasers of 561 nm and 640 nm were reflected by a quad dichroic and the emission was filtered by a quad emission filter (open at 581 – 625 nm and 674 – 786 nm). The images were captured using an SR HP APO TIRF 100× 1.49 NA objective (Nikon) and an iXon Ultra 897 EMCCD camera (Andor). CF568 and JF646 fluorophores were converted into a dark state using continuous illumination of excitation light at the maximum intensity. 405 nm laser at low intensity was used to activate fluorophores back to a fluorescent state. Individual blinking CF568 and JF646 fluorophores were recorded for 30,000 to 50,000 frames with 30 milliseconds exposure time. 100 nm Red Fluorescent Nanodiamond (Adámas Nanotechnologies, NDNV100nmHi2ml) was used as a fiducial marker for drift correction. Images were analyzed by ThunderSTORM plug-in[86] on ImageJ (Fiji), and rendered with an

average shifted histogram method. Colocalization between CD28 and B7, or between CD28 and PDL1, was quantified by Manders coefficients using the Coloc-Tesseler software.[87]

Jurkat:Raji Cell Coculture Assay—For Figure 2 and Figure S2 A, B, D, to allow for discrimination of Raji cells and reporter Jurkat cells in the coculture, Raji cells were pre-labeled with VF405 (Biotium, 30068) following manufacturer's instructions. The labeled Raji cells were incubated with 30 ng/mL SEE for 30 min at 37 °C. 1.8×10^6 VF405-labeled, SEE-loaded Raji cells were then co-pelleted with 1.8×10^4 Jurkat cells in a 24-well plate and incubated at 37 °C, 5% CO_2 for 16 h. For abatacept treated conditions, Jurkat cells were pre-incubated with 20 μg/mL abatacept for 1 h before co-pelleting with Raji cells. After 16 h coculture, GFP (NFκB) and mCherry (AP1) expression in VF405- cells (Jurkat) were examined using a BD LSRFortessa X-20 flow cytometer. Meanwhile, IL-2 concentrations in the supernatants were measured using the Human IL-2 ELISA MAX Deluxe kit (BioLegend, 431804). For Figure S2C, 1.8×10^4 Jurkat ($CD28^{-/-}$) cells, Jurkat ($CD28^{+/+}$) cells, Jurkat ($CD28^{-/-} CD80^+$) cells, Jurkat ($CD28^{+/+}CD80^+$) cells, Jurkat ($CD28^{-/-}CD86^+$) cells, or Jurkat ($CD28^{+/+}CD86^+$) cells were mixed with 1.8×10^6 SEE-loaded Raji ($CD80^{-/-}CD86^{-/-}$) cells. Jurkat cells and Raji cells were co-pelleted in a 24-well plate and incubated at 37 °C, 5% CO_2 for 6 h. IL-2 concentrations in the supernatants were measured using the Human IL-2 ELISA MAX Deluxe kit (BioLegend).

For Figure 4E, 1.8×10^4 *CD28(WT)$^+$CD80$^+$* Jurkat cells, *CD28(Y191F)$^+$CD80$^+$* Jurkat cells, *CD28(CD45TM)$^+$CD80$^+$* Jurkat cells, *CD28(WT)$^+$CD86$^+$* Jurkat cells, *CD28(Y191F) $^+$CD86$^+$* Jurkat cells, or *CD28(CD45TM)$^+$CD86$^+$* Jurkat cells were mixed with 1.8×10^6 SEE-loaded *CD80$^{-/-}$CD86$^{-/-}$* Raji cells. For Figure 4F, 1.8×10^4 *CD28(WT)$^+$* Jurkat cells, *CD28(Y191F)$^+$* Jurkat cells, or *CD28(CD45TM)$^+$* Jurkat cells were mixed with 1.8×10^6 SEE-loaded *CD80$^{+/+}$CD86$^{-/-}$* Raji cells (providing *trans*-CD80) or *CD80$^{-/-}$CD86$^{+/+}$* Raji cells (providing *trans*-CD86). For *cis*-signaling groups in Figure 5B, 1.8×10^4 *CD28(WT) $^+$CD80-CLIP$^+$* Jurkat cells, *CD28(Y191F)$^+$CD80-CLIP$^+$* Jurkat cells, or *CD28(Y209F) $^+$CD80-CLIP$^+$* Jurkat cells were mixed with 5.4×10^5 SEE-loaded *CD80$^{-/-}$CD86$^{-/-}$* Raji cells. For *trans*-signaling groups in Figure 5B, 1.8×10^4 *CD28(WT)$^+$* Jurkat cells, *CD28(Y191F)$^+$* Jurkat cells, or *CD28(Y209F)$^+$* Jurkat cells were mixed with 5.4×10^5 SEE-loaded *CD80$^{+/+}$CD86$^{-/-}$* Raji cells (providing *trans*-CD80). For Figure 6D, 1.8×10^4 *SNX9$^{+/+}$*Jurkat cells, *SNX9$^{+/+}$CD80$^+$CD86$^+$*Jurkat cells, or *SNX9$^{-/-}$CD80$^+$CD86$^+$*Jurkat cells were each mixed with 1.8×10^6 SEE-loaded *CD80$^{-/-}$CD86$^{-/-}$* Raji cells. For IL-2 readouts, Jurkat cells and Raji cells were co-pelleted in a 24-well plate and incubated at 37 °C, 5% CO_2, 6 h later, IL-2 concentration in the medium were measured using the Human IL-2 ELISA MAX Deluxe kit (BioLegend). IL-2 secretion in Figure 5B was normalized to that of Jurkat cells expressing WT CD28.

For Figure 5A and Figure 6C, 3×10^5 Jurkat cells were co-pelleted with 1.5×10^6 SEE-loaded Raji cells at $300 \times g$ for 1 min, and then incubated in culture medium at 37 °C, 5% CO_2 for 30 min. Cells were then resuspended, fixed with 4% PFA and permeabilized with 0.1% saponin (MilliporeSigma, 558255). Afterward, CD28 was stained by AF647-labeled anti-CD28 (BioLegend, 302953), PKCθ was stained by anti-PKCθ (Cell Signaling, 13643S) and then by CF568-conjugated anti-rabbit IgG antibody (Biotium, 20801). Stained cells were loaded into a 96-well glass-bottom plate for confocal microscopy assays. Images were

acquired with a Leica SP8 confocal microscope and processed, and quantified using ImageJ. To calculate the synaptic enrichment indices of CD28 and PKCθ, the fluorescence density at the interface was divided by the fluorescence density of the cell excluding the interface. Fluorescence density was calculated as fluorescence intensity divided by area. The interface was defined as the conjugate area between Jurkat and Raji cells based on the DIC images and the fluorescence channels. Imaging fields were randomly selected under the confocal microscope and all the Jurkat:Raji cell conjugates with each recorded imaging field were analyzed. Reported data were pooled from at least three independent experiments.

BiLC Assay—For measurement of ICD proximity in Figure 3D, HEK293T cells were co-transfected with a pHR plasmid encoding *CD80* or *CD86* fused to a C-terminal SmBiT and a pHR plasmid encoding *CD28* or *CD274* (PDL1) fused to a C-terminal LgBiT. 20 h post transfection, 1×10^5 cells were trypsinized and seeded in a 96-well solid white microplate (Greiner Bio-One, 655075) in Opti-MEM I medium (ThermoFisher, 31985070). For measurement of ECD proximity in Figure 3E, HEK293T cells were co-transfected with a pHR plasmid encoding *CD80* or *CD86* fused to a N-terminal SmBiT and a pHR plasmid encoding *CD28* or *CD274* (PDL1) fused to a N-terminal SpyTag. We used the SpyTag:SpyCatcher system to recruit soluble LgBiT-SpyCatcher fusion protein to Spy-CD28 or Spy-PDL1 expressed on the cell surface due to abnormal cytosolic localization caused by LgBiT fusion to CD28 ECD. For *trans*-interaction control in Figure 3F, HEK293T cells were transfected by *CD28* fused with an N-terminal SpyTag, *CD80* fused with an N-terminal SmBiT, or *CD86* fused with an N-terminal SmBiT. 20 h later, 1×10^5 cells were treated with 20 nM purified LgBiT-SpyCatcher protein at 37 °C for 1 h to label Spy-CD28. Single transfected cells were mixed at an equal ratio immediately before the addition of LgBiT-SpyCatcher and used as *trans*-interaction control. For abatacept and atezolizumab treated conditions, cells were pretreated with 20 μg/mL abatacept or atezolizumab (Bio X Cell, SIM0009) before subjected to the LgBiT-SpyCatcher labeling. Labeled cells were then incubated with 20 μM furimazine (Aobious, AOB36539) and luminescence measured using a Tecan Spark 20 plate reader. In Figure S3, expression of Spy-CD28, SmBiT-CD80, or SmBiT-CD86 in single- or double-transfected HEK293T cells were determined by flow cytometry after staining the cells with PE anti-CD28 (BioLegend, 302940), allophycocyanin anti-CD80 (BioLegend, 305220), or allophycocyanin anti-CD86 (BioLegend, 374207). The antibody-stained double-transfected cells were also observed using a Leica SP8 microscope and the percentages of isolated *Spy-CD28*^{+}*SmBiT-B7*[+] double positive cells were calculated from randomly selected confocal images.

Protein Docking—To predict the structures of human CD80:CD28 and CD86:CD28 complexes, CD28 (PDB: 1YJD), CD80 (PDB: 1DR9), and CD86 (PDB: 1NCN) were docked using ClusPro 2.0.[88–91] Because CD28 and CTLA4 share the conserved MYPPPY motif for B7 binding, we used CD28 MYPPPY motif and previously identified CTLA4-MYPPPY-binding residues in B7[92,93] to guide B7:CD28 docking. Specifically, Y65, M72, T75, M77, V117, L119, A125, F126 and L131 from CD80 were used for CD80:CD28 docking; V54, F56, Q58, N62, L63, V64, E67, Y69, K74, S77, I111, H113, M120, and R122 of CD86 were used for CD86:CD28 docking. These residues and the MYPPPY residues in CD28 were used as attraction residues in ClusPro 2.0 to predict structures,

which were then ranked based on cluster size. The structures with the largest cluster size were shown in Figure 3B.[90] CD86 Ig-like C2 domain was predicted by AlphaFold[94] and downloaded from Uniprot (https://www.uniprot.org/uniprotkb/P42081/entry#structure).

Internalization Assay of CD28 Variants—To probe CD28 endocytosis in Figure 4C, we fused its ECD with a SpyTag for monovalent labeling by SpyCatcher, avoiding crosslinking-induced endocytosis as seen with antibody staining. *CD28⁻/⁻* Jurkat cells were transduced with *CD28(WT), CD28(Y191F)*, or *CD28(CD45TM)* fused with an N-terminal SpyTag, and stained with biotinylated SpyCatcher on ice for 30 min. Labeled cells were then incubated either on ice to prevent endocytosis or at 37 °C to restore endocytosis. Aliquots were collected at the indicated times, CD28 remained on the cell surface were labeled with AF647-conjugated streptavidin on ice, and analyzed by flow cytometry for AF647 fluorescence. The AF647 fluorescence of samples collected at 0 min were used as references (100%) to calculate the percentages of surface CD28 at other time points. For confocal imaging, Jurkat cells expressing each of the indicated Spy-CD28 variant were stained with JF646*SpyCatcher on ice, and then incubated for 60 min at 37 °C or on ice, followed by fixation with 4% PFA and confocal microscopy.

Subcellular Localization of *Cis*-complexes Using TEM—For Figure 4G, *CD28⁻/⁻* Jurkat cells were lentivirally co-transduced with *CD28* or *CD274* (PDL1) fused with an N-terminal ALFA-tag and *CD80* or *CD86* fused with an N-terminal SpyTag. Transduced Jurkat cells were labeled with EX-NbALFA and AP-SpyCatcher at 37 °C for 30 min, and washed twice with culture medium to remove unbound proteins. Labeled cells were incubated in culture medium containing 5 μM Hemin (Sigma, 51280) at 37 °C for 2 h, and seeded on a poly-D-lysine-coated coverslip and stained with DAB solution (0.5 mg/mL DAB and 10 mM H_2O_2 in culture medium) at 37 °C for 30 min. Stained cells were then fixed with 2% glutaraldehyde in 0.1 M sodium cacodylate buffer (0.1 M sodium cacodylate, 2 mM $CaCl_2$, pH 7.4) at 37 °C for 30 sec, followed by buffer exchange with fresh fixation buffer for 3 times. Cells were kept in the fixation buffer at 4 °C overnight and then embedded in Ducurpan. Specifically, cells were washed for 3 min in 0.1 M sodium cacodylate buffer and repeated 4 times. Washed cells were stained by 1% OsO4 in 0.1 M sodium cacodylate buffer for 30 – 60 min, followed by 5 washes with 0.1 M sodium cacodylate buffer and 1 time wash in ddH_2O. Stained cells were subjected to dehydration through incubating for 1 min in each of following solutions containing increasing ethanol (volume to volume percentage): 20%, 50%, 70%, 90%, 100%, 100%, and then for 2×1 min in 100% acetone. Dehydrated cells were infiltrated in an equal volume mixture of Ducurpan and acetone for 1 h and then twice in 100% Durcupan for 1 h each. Embedded cells were incubated in foil plates along with wood sticks in embedding oven for overnight. 60 nm ultrathin sections were cut with a diamond knife and mounted on 300 mesh grids for TEM. Grids were then stained with 2% of uranyl acetate for 5 min and lead citrate for 1 min. Images were acquired using a JEOL 1400 plus transmission electron microscope.

Jurkat:SLB Microscopy Assay—For Figure 6E, SLB was prepared in a glass-bottom 96-well plate (Cellvis, P96–1.5H-N), which was first incubated with 5% HellmanexIII (Helma Analytics, Z805939) overnight on a 50 °C heat pad, thoroughly rinsed with ddH2O

and sealed with a Nunc sealing tape (Thermo Fisher Scientific, 232698). The desired wells were washed twice with 5 M NaOH (60 min each), and thrice with ddH$_2$O followed by equilibration with 1x PBS. Small unilamellar vesicles (SUVs, consisting of 95.5% POPC, 2% DGS-NTA-Ni, 2% biotin-DPPE, and 0.5% PEG5000 PE) were prepared as described previously,[95] added to the cleaned wells containing 200 μL 1x PBS, and incubated for 90 min at 50 °C, followed by 30 min at 37 °C to induce SLB formation. The wells were then rinsed thoroughly with 1x PBS to remove excess SUVs. The resulting SLBs were incubated with 1 μg/ml streptavidin (ThermoFisher Scientific, S888) and 10 nM His-tagged human ICAM1 ECD (Sino Biological, 10346-H08H) at 37 °C for 1 h. Afterward, the SLBs were rinsed with 1x PBS and further incubated with 5 μg/ml biotin anti-human-CD3ε (BioLegend, 317320) at 37 °C for 30 min, followed by three rinses with 1x PBS and three rinses with imaging buffer (20 mM HEPES-NaOH, pH 7.5, 137 mM NaCl, 5 mM KCl, 1 mM CaCl$_2$, 2 mM MgCl$_2$, 0.7 mM Na$_2$HPO$_4$, 6 mM D-glucose). Jurkat cell membranes were stained by 2 μM R18 on ice for 5 min, followed by two rinses with ice-cold 1x PBS. Stained cells were then resuspended in imaging buffer and plated onto SLBs. After 30 min incubation at 37 °C, cells were fixed with 4% PFA at room temperature for 15 min. SLB-associated, PFA-treated cells were washed with blocking buffer (1× PBS containing 3% BSA), and permeabilized with 1× PBS containing 3% BSA and 0.1% saponin at room temperature for 60 min. Cells were then stained with AF647 anti-CD28 (BioLegend, 302953). Z-stack airyscan confocal images were acquired using a Zeiss LSM 880 confocal microscope.

Primary T cell Assay—For Figure 2B, splenocytes from 6–12 weeks old WT C57BL/6J mice (2 male, 1 female) or *Cd80*$^{-/-}$*Cd86*$^{-/-}$ C57BL/6J mice (2 male, 1 female) were cultured in 6-well plates that were pre-coated with 5 μg/mL anti-CD3ε antibody (BioLegend, 100340). 1 μg/mL anti-CD28 antibody (BioLegend, 102116) and 100 U/mL human IL-2 (PeproTech, 200–02) were supplemented in culture medium. After 3-day activation, cells were collected by centrifuge and cultured in new plates using primary T cell medium containing 100 U/mL IL-2. On day 4, CD28, CD80, and CD86 expression were measured on CD4$^+$ and CD8$^+$ T cells using flow cytometry. Live cells were collected through a density gradient centrifugation of Histopaque 1077 (Sigma, 10771), followed by purification of T cells using mouse CD3 T cell isolation kit (BioLegend, 480031). To measure IFNγ production, 2×10^5 purified T cells were stimulated with 5×10^6 irradiated (3400 rad) *Cd80*$^{-/-}$*Cd86*$^{-/-}$ splenocytes, which were pre-loaded with 1 μg/mL anti-CD3ε antibody (BioLegend, 100340) and pre-stained with VF405. Cells were cultured in primary T cell medium with 5 μg/mL brefeldin A (BioLegend, 420601) for 6 h, and then incubated with Zombie Aqua viability dye (BioLegend, 423102), followed by staining with FITC anti-mouse CD4 (BioLegend, 100510) and PerCP/Cyanine5.5 anti-mouse CD8 (BioLegend, 100734). Cells were then fixed by 4% PFA and permeabilized with 0.05% TritonX-100. Fixed cells were further stained with a mixture of antibodies containing allophycocyanin-Cy7 anti-mouse CD3ε (BioLegend,100330) and BV711 anti-mouse IFNγ (BioLegend, 505835). Cells were processed on a BD LSRFortessa X20 by BD FACSDiva software (BD Biosciences) and data analyzed using FlowJo. CD4$^+$ and CD8$^+$ T cells were identified as VF405$^-$CD4$^+$CD3$^+$ and VF405$^-$CD8$^+$CD3$^+$ population respectively.

For Figure 2C, PBMCs were isolated from human white blood cells (San Diego Blood Bank) through a density gradient of Histopaque 1077 (Sigma, 10771). Human PBMCs were then cultured in primary T cell medium supplemented with 50 U/mL human IL-2 and 1 μg/mL SEB (Toxin Technology, BT202). After 3-day priming, cells were collected by centrifuge and further cultured in primary T cell medium supplemented with 50 U/mL human IL-2 but no SEB. After another 24 h, CD28, CD80, and CD86 expression were measured on $CD4^+$ and $CD8^+$ T cells using flow cytometry. Live cells were collected through a density gradient of Histopaque 1077 (Sigma, 10771). To measure IFNγ production, 1×10^5 purified T cells were stimulated with 3.6×10^6 $CD80^{-/-}CD86^{-/-}$ Raji cells pre-loaded with 1 μg/mL SEB and pre-stained with VF405. Cells were cultured in primary T cell medium with 5 μg/mL brefeldin A (BioLegend, 420601) for 6 h. Cells were then incubated with Zombie Aqua viability dye (BioLegend, 423102), followed by staining with FITC anti-human CD4 (BioLegend, 317408) and PerCP-Cy5.5 anti-human CD8 (BioLegend, 301031). Cells were then fixed by 4% PFA and permeabilized with 0.05% TritonX-100. Fixed cells were further stained with a mixture of antibodies containing AF700 anti-human CD3ε (BioLegend, 317340), PE anti-human CD80 (BioLegend, 305208), PE anti-human CD86 (BioLegend, 374206), and BV711 anti-human IFNγ (BioLegend, 502539). Stained cells were processed on a BD LSRFortessa X20 by BD FACSDiva software (BD Biosciences) and analyzed using FlowJo. $CD4^+$ and $CD8^+$ T cells were identified as $VF405^-CD4^+CD3^+$ and $VF405^-CD8^+CD3^+$ population respectively. $B7^+$ T cells, expressing CD80, CD86 or both, were gated identified as the PE+ population. To measure CD69 expression in Figure S2E, 1×10^5 purified T cells were stimulated with 3.6×10^6 VF405-stained $CD80^{-/-}CD86^{-/-}$ Raji cells in the presence or absence of 1 μg/mL SEB. After 6 h coculture, cells were then incubated with Zombie Aqua viability dye (BioLegend, 423102), followed by staining with an antibody mixture containing FITC anti-human CD4 (BioLegend, 317408) and PerCP-Cy5.5 anti-human CD8 (BioLegend, 301031), AF700 anti-human CD3ε (BioLegend, 317340), PE anti-human CD80 (BioLegend, 305208), PE anti-human CD86 (BioLegend, 374206), and allophycocyanin anti-human CD69 (BioLegend, 310909).

OT-1 cell culture assays—For Figure 1A and Figure S1, splenocytes from 6–12 weeks old OT-1 mice were cultured in primary T cell medium containing 100 U/mL human IL-2 (PeproTech, 200–02) and 10 nM $OVA_{257-264}$ (Anaspec, AS-60193–1) at 37 °C, 5% CO_2. CD28, CD80 and CD86 expression on $CD8^+$ T cells, identified as $CD3^+CD8^+$ cells, were measured by flow cytometry at indicated times. Briefly, cells were pre-stained with viability dye Zombie Violet (BioLegend, 423113), and then incubated with TruStain FcX plus (BioLegend, 156604) to block Fc receptors, followed by an antibody mixture containing allophycocyanin-Cy7 anti-mouse CD3ε (BioLegend,100330), FITC anti-mouse CD8 (BioLegend, 140404), PE anti-mouse CD80 (BioLegend, 104707), APC anti-mouse CD86 (BioLegend, 105011), and PE-Cy7 anti-mouse CD28 (BioLegend, 102126). Stained cells were processed on a BD LSRFortessa cell analyzer and flow cytometry data analyzed by FlowJo software.

For Figure 7A, B, and E, OT-1 T cells were primed as in Figure 1A. After 4 days of priming, live cells were collected through a density gradient of Histopaque 1077 (Sigma,

10771). Live OT-1 T cells were treated with 20 μg/mL abatacept or control IgG (Bio X Cell, BE0096) at 37 °C for 1 h. 6×10^4 IgG or abatacept treated OT-1 T cells were then cultured with 3×10^5 VF405-labeled irradiated B16F10 or B16OVA cells (8000 rad). IgG or abatacept was also included at 20 μg/mL in the coculture medium. After 24 h coculture, medium was collected for IL-2 (BioLegend, 431001) and IFNγ (BioLegend, 430801) measurement using ELISA, and cells were collected for GzmB and Ki67 staining. After 72 h culturing, OT-1 T cells viability and Bcl-xL expression were analyzed. Briefly, cells were incubated with Zombie Aqua viability dye (BioLegend, 423102), followed by FITC anti-mouse CD8 (BioLegend, 140404) staining. Stained cells were fixed with 4% PFA and permeabilized with 0.05% Triton X-100. Permeabilized cells were then stained with PE anti-mouse GzmB (BioLegend, 372207), PE-Cy7 anti-mouse Ki67 (BioLegend, 652425), and anti-Bcl-xL (Proteintech, 10783–1-AP) followed by AF647 anti-rabbit IgG (BioLegend, 406414) staining. Stained cells were processed on a BD LSRFortessa or LSRFortessa X20 cell analyzer and flow cytometry data analyzed by FlowJo.

For Figure 7C, OT-1 T cells were primed as in Figure 1A except that cells were split on day 3 and cultured in the presence of either 100 U/mL human IL-2 (PeproTech, 200–02) or 10 ng/mL human IL-15 (PeproTech, 200–15) for another 3 days. Afterward, live cells were collected through a density gradient of Histopaque 1077. Live OT-1 T cells were then incubated in migration buffer (RPMI 1640 [ThermoFisher, 11835030] supplemented with 0.1% FBS, 1 mM sodium pyruvate, 50 mM β-mercaptoethanol, 100 U/mL of Penicillin, and 100 mg/mL of Streptomycin) for 4 h before added into a transwell inserts (Corning, 3421) pre-coated with 10 μg/mL FN (Corning, 354008), in the presence of 20 μg/mL abatacept or control IgG in migration buffer. 1×10^6 T cells were added into each insert. 4 h later, the number of T cells in the bottom well was quantified using an EVE cell counter (NanoEntek).

For Figure 7D, OT-1 cells were primed as in Figure 7C in the presence IL-15. OT-1 cells after 24 h priming were retrovirally transduced with LifeAct-mCherry as previously described.[96] After 6 days priming, T cells expressing LifeAct-mCherry, sorted using flow cytometry, were incubated in migration buffer for 4 h in the presence of 20 μg/mL abatacept or control IgG. Treated cells were seeded onto a glass-bottom 96-well plate, which was pre-coated with 2 μg/mL mouse ICAM1 (Sino Biological, 50440-M08H). After incubation at 37°C for 20 min, cells were fixed by 4% PFA and actin foci were observed through TIRF microscopy.

For Figure 7J, CD8+ naïve T cells were isolated from *Cd28*$^{-/-}$ OT-1 mice using mouse CD8 naïve T cell isolation kit (BioLegend, 480044) and activated with plate-bound anti-CD3ε antibodies (5 μg/mL, BioLegend, 100340) in primary T cell media containing 100 U/mL human IL-2. Cells were transduced twice at 24 h and 48 h using retrovirus produced by Platinum-E cells co-transfected with pCl-Eco packaging plasmid and pQCX plasmid encoding *Cd28(WT)* or *Cd28(Y170F)*. At 96 h, cells were cocultured with VF405-labeled irradiated B16F10 cells preloaded with 30 pM OVA$_{257-264}$, in the presence of 20 μg/mL abatacept or control IgG. After 24 h coculture, medium was collected for IL-2 (BioLegend, 431001) and IFNγ (BioLegend, 430801) ELISA, and cells were collected for GzmB staining and flow cytometry measurement as mentioned above.

For Figure S7D, *Cd28*$^{-/-}$ OT-1 cells were isolated, activated, and transduced as in Figure 7J, except LifeAct-mCherry was co-transduced. After 3-day priming, OT-1 cells were cultured in primary T cell media containing 10 ng/mL human IL-15 (PeproTech, 200–15) for another 3 days. Actin foci were detected as in Figure 7D.

OT-1 cell adoptive transfer and B16OVA tumor growth assays—For B16OVA tumor growth experiment in Figure 7F–I, 8–12 weeks old male and female C57BL/6J *CD80*$^{-/-}$*CD86*$^{-/-}$ mice, which were distributed across multiple cages and litters, were inoculated with 2.5×10^5 B16OVA cells in the subcutaneous space. Five days later, mice were intravenously injected with 5×10^6 OT-1 T cells, which were primed for 4 days as described in Figure 1A and collected through a density gradient of Histopaque 1077 for live cells. 200 μg abatacept or control IgG was intraperitoneally injected twice per week from the day 5 post tumor inoculation. Abatacept and IgG treatment were randomly applied to both male and female mice. The tumor volume (V) was estimated using: $V = ab^2/2$, in which *a* denotes the longer diameter and *b* denotes the shorter diameter. Tumor and blood were harvested from all animals after 26 or 29 days of tumor inoculation. Tumor samples were treated by collagenase (Worthington Biochemical, LS004197) and soybean trypsin inhibitor (Worthington Biochemical, LS003587) at 37°C for 30 min to prepare single cell suspensions. For cytokine measurement, single cell suspensions of tumors were further cultured in primary T cell medium supplementing with 10 nM OVA$_{257-264}$ and 5 μg/mL brefeldin A (BioLegend, 420601) for 6 h. Single cell suspensions were pre-incubated with the viability dye Zombie Aqua, and then incubated with TruStain FcX plus (BioLegend, 156604) to block Fc receptors, followed by BV421 OVA$_{257-264}$ H-2K^b tetramer (NIH) staining. Cells were further stained with a mixture of antibodies containing anti-CD45 (BioLegend, 103149), anti-CD8 (Bio-Rad, MCA609SBV610; Accurate Chemical, ACL168F), anti-CD62L (BioLegend, 104448), anti-CD44 (BioLegend, 103049), anti-CD80 (BioLegend, 104743), anti-CD86 (BioLegend, 105011), anti-PD1 (BioLegend, 109104), anti-IFNγ (BioLegend, 505835), and anti-TNFα (BioLegend, 506315), each conjugated to a different fluorochrome. Cells were processed on a BD LSRFortessa X20 by BD FACSDiva software (BD Biosciences). OT-1 T cells were identified by positive staining with OVA$_{257-264}$-H-2K^b tetramer in the live, CD45$^+$CD8$^+$ population. Data obtained were analyzed using FlowJo.

For Figure 7K–N, 8–10 weeks old male and female WT C57BL/6J mice, distributed across multiple cages and litters, were inoculated with 2.5×10^5 B16OVA cells in the subcutaneous space. Five days later, mice were intravenously injected with 5×10^6 *Cd28(WT)*$^+$ OT-1 T cells, 5×10^6 *Cd28(Y170F)*$^+$ OT-1 T cells, or PBS alone. *Cd28(WT)*$^+$ and *Cd28(Y170F)*$^+$ OT-1 T cells were generated as in Figure 7J and proliferated for another 2 days in primary T cell media containing 100 U/mL IL-2 after 3-day priming. Before injection, live OT-1 cells were collected through a density gradient of Histopaque 1077. Tumor growth was measured blindly twice per week and volume was calculated as in Figure 7F. Tumor and blood were harvested from all animals after 23, 26 or 29 days of tumor inoculation. OT-1 T cells in tumor and blood and cytokine production were measured as in Figure 7G–I.

For Figure S5, B16F10 and B16OVA were cultured for 24 h in the presence of mouse IFNγ at the indicated concentration, followed by measurement of CD80, CD86, and PDL1 expression using a BD LSRFortessa.

For immunohistochemistry analysis in Figure S6, 21 B16OVA tumors from IgG and Abata treated mice in Figure 7F were fixed in formalin for 24 h and kept in 70% ethanol, followed by paraffin embedding. Sectioned tissues were baked at 60 °C for 1 h, followed by rehydration through successive treatment in Xylene (thrice), 100% ethanol (twice), 95% ethanol (twice), 70% ethanol (twice) and ddH$_2$O. Antigen retrieval was performed in Antigen Unmasking Solution (Citrate Based, pH 6) (Vector, H-3300) at 95 °C for 30 min. Staining was performed on an Intellipath Automated IHC Stainer (Biocare). Peroxidase was blocked with Bloxall (Vector, SP-6000) for 10 min. Tissues were blocked with 3% Donkey Serum for 10 min, followed by staining with anti-CD3ε Primary Antibody (Rabbit, Abcam, ab16669, 1:100) for 1 h, anti-Rabbit HRP Polymer (Cell IDX, 2RH-100) for 30 min, and Tyramide-488 Reagent (ThermoFisher Scientific, B40953) for 10 min. Stained tissue sections were mounted with Vectashield Vibrance containing DAPI (Vector, H-1800–10) and observed using a Leica SP8 confocal microscope. 10 random selected areas from each sample were used to count isolated CD3$^+$ cells.

QUANTIFICATION AND STATISTICAL ANALYSIS

Data were shown as mean ± SEM, and number of replicates were indicated in Figure legends. Statistical significance was evaluated by two-tailed Student's t test, One-way ANOVA, or Two-way ANOVA (*, $p < 0.05$; **, $p < 0.01$; ***, $p < 0.001$; ****, $p < 0.0001$) in GraphPad Prism 9. Data with $p > 0.05$ are considered statistically non-significant (ns).

Supplementary Material

Refer to Web version on PubMed Central for supplementary material.

Acknowledgments

References

1. Hansen JA, Martin PJ, and Nowinski RC (1980). Monoclonal antibodies identifying a novel T-Cell antigen and Ia antigens of human lymphocytes. Immunogenetics 10, 247–260. 10.1007/BF01561573.

2. Gmünder H, and Lesslauer W (1984). A 45-kDa human T-cell membrane glycoprotein functions in the regulation of cell proliferative responses. Eur J Biochem 142, 153–160. 10.1111/j.1432-1033.1984.tb08263.x. [PubMed: 6235110]

3. Esensten Jonathan H., Helou Ynes A., Chopra G, Weiss A, and Bluestone Jeffrey A. (2016). CD28 Costimulation: From Mechanism to Therapy. Immunity 44, 973–988. 10.1016/j.immuni.2016.04.020. [PubMed: 27192564]

4. Boomer JS, and Green JM (2010). An enigmatic tail of CD28 signaling. Cold Spring Harbor perspectives in biology 2, a002436. 10.1101/cshperspect.a002436. [PubMed: 20534709]

5. Weng N-P, Akbar AN, and Goronzy J (2009). CD28(−) T cells: their role in the age-associated decline of immune function. Trends Immunol 30, 306–312. 10.1016/j.it.2009.03.013. [PubMed: 19540809]

6. Fagnoni FF, Vescovini R, Mazzola M, Bologna G, Nigro E, Lavagetto G, Franceschi C, Passeri M, and Sansoni P (1996). Expansion of cytotoxic CD8+ CD28− T cells in healthy ageing people, including centenarians. Immunology 88, 501–507. 10.1046/j.1365-2567.1996.d01-689.x. [PubMed: 8881749]

7. Saurwein-Teissl M, Lung TL, Marx F, Gschösser C, Asch E, Blasko I, Parson W, Böck G, Schönitzer D, Trannoy E, and Grubeck-Loebenstein B (2002). Lack of antibody production following immunization in old age: association with CD8(+)CD28(−) T cell clonal expansions and an imbalance in the production of Th1 and Th2 cytokines. J Immunol 168, 5893–5899. 10.4049/jimmunol.168.11.5893. [PubMed: 12023394]

8. Zang X, and Allison JP (2007). The B7 Family and Cancer Therapy: Costimulation and Coinhibition. Clinical Cancer Research 13, 5271–5279. 10.1158/1078-0432.Ccr-07-1030. [PubMed: 17875755]

9. Porciello N, Kunkl M, and Tuosto L (2018). CD28 between tolerance and autoimmunity: the side effects of animal models. F1000Res 7, F1000 Faculty Rev-1682. 10.12688/f1000research.14046.1.

10. Filion LG, Matusevicius D, Graziani-Bowering GM, Kumar A, and Freedman MS (2003). Monocyte-derived IL12, CD86 (B7–2) and CD40L expression in relapsing and progressive multiple sclerosis. Clinical Immunology 106, 127–138. 10.1016/S1521-6616(02)00028-1. [PubMed: 12672403]

11. Borowski AB, Boesteanu AC, Mueller YM, Carafides C, Topham DJ, Altman JD, Jennings SR, and Katsikis PD (2007). Memory CD8+ T Cells Require CD28 Costimulation. The Journal of Immunology 179, 6494–6503. 10.4049/jimmunol.179.10.6494. [PubMed: 17982038]

12. Harding FA, McArthur JG, Gross JA, Raulet DH, and Allison JP (1992). CD28-mediated signalling co-stimulates murine T cells and prevents induction of anergy in T-cell clones. Nature 356, 607–609. 10.1038/356607a0. [PubMed: 1313950]

13. Kamphorst AO, Wieland A, Nasti T, Yang S, Zhang R, Barber DL, Konieczny BT, Daugherty CZ, Koenig L, Yu K, et al. (2017). Rescue of exhausted CD8 T cells by PD-1–targeted therapies is CD28-dependent. Science 355, 1423–1427. 10.1126/science.aaf0683. [PubMed: 28280249]

14. Sharpe AH, and Freeman GJ (2002). The B7–CD28 superfamily. Nature Reviews Immunology 2, 116–126. 10.1038/nri727.

15. Azuma M, Yssel H, Phillips JH, Spits H, and Lanier LL (1993). Functional expression of B7/BB1 on activated T lymphocytes. J Exp Med 177, 845–850. 10.1084/jem.177.3.845. [PubMed: 7679711]

16. Jeannin P, Herbault N, Delneste Y, Magistrelli G, Lecoanet-Henchoz S, Caron G, Aubry J-P, and Bonnefoy J-Y (1999). Human Effector Memory T Cells Express CD86: A Functional Role in Naive T Cell Priming. The Journal of Immunology 162, 2044–2048. 10.4049/jimmunol.162.4.2044. [PubMed: 9973476]

17. Hwang I, Huang JF, Kishimoto H, Brunmark A, Peterson PA, Jackson MR, Surh CD, Cai Z, and Sprent J (2000). T cells can use either T cell receptor or CD28 receptors to absorb and internalize cell surface molecules derived from antigen-presenting cells. J Exp Med 191, 1137–1148. 10.1084/jem.191.7.1137. [PubMed: 10748232]

18. Radziewicz H, Ibegbu CC, Hon H, Bédard N, Bruneau J, Workowski KA, Knechtle SJ, Kirk AD, Larsen CP, Shoukry NH, and Grakoui A (2010). Transient CD86 expression on hepatitis C

virus-specific CD8+ T cells in acute infection is linked to sufficient IL-2 signaling. Journal of immunology 184, 2410–2422. 10.4049/jimmunol.0902994.

19. Cross AH, Lyons JA, San M, Keeling RM, Ku G, and Racke MK (1999). T cells are the main cell type expressing B7–1 and B7–2 in the central nervous system during acute, relapsing and chronic experimental autoimmune encephalomyelitis. European Journal of Immunology 29, 3140–3147. 10.1002/(SICI)1521-4141(199910)29:10<3140::AID-IMMU3140>3.0.CO;2-W. [PubMed: 10540325]

20. Abe K, Takasaki Y, Ushiyama C, Asakawa J, Fukazawa T, Seki M, Hirashima M, Ogaki M, and Hashimoto H (1999). Expression of CD80 and CD86 on Peripheral Blood T Lymphocytes in Patients with Systemic Lupus Erythematosus. Journal of Clinical Immunology 19, 58–66. 10.1023/a:1020566618980. [PubMed: 10080105]

21. Sun Z. w., Qiu Y. h., Shi Y. j., Tao R, Chen J, Ge Y, Hu Y. m., Ma H. b., Shi Q, and Zhang X. g. (2005). Time courses of B7 family molecules expressed on activated T-cells and their biological significance. Cellular Immunology 236, 146–153. 10.1016/j.cellimm.2005.08.021. [PubMed: 16165113]

22. Stephan MT, Ponomarev V, Brentjens RJ, Chang AH, Dobrenkov KV, Heller G, and Sadelain M (2007). T cell–encoded CD80 and 4–1BBL induce auto- and transcostimulation, resulting in potent tumor rejection. Nature Medicine 13, 1440–1449. 10.1038/nm1676.

23. Keeble AH, Turkki P, Stokes S, Khairil Anuar INA, Rahikainen R, Hytönen VP, and Howarth M (2019). Approaching infinite affinity through engineering of peptide–protein interaction. Proceedings of the National Academy of Sciences 116, 26523–26533. 10.1073/pnas.1909653116.

24. Jutz S, Leitner J, Schmetterer K, Doel-Perez I, Majdic O, Grabmeier-Pfistershammer K, Paster W, Huppa JB, and Steinberger P (2016). Assessment of costimulation and coinhibition in a triple parameter T cell reporter line: Simultaneous measurement of NF-κB, NFAT and AP-1. Journal of Immunological Methods 430, 10–20. 10.1016/j.jim.2016.01.007. [PubMed: 26780292]

25. Kariv I, Truneh A, and Sweet RW (1996). Analysis of the site of interaction of CD28 with its counter-receptors CD80 and CD86 and correlation with function. J Immunol 157, 29–38. 10.4049/jimmunol.157.1.29. [PubMed: 8683128]

26. Peach RJ, Bajorath J, Naemura J, Leytze G, Greene J, Aruffo A, and Linsley PS (1995). Both extracellular immunoglobin-like domains of CD80 contain residues critical for binding T cell surface receptors CTLA-4 and CD28. Journal of Biological Chemistry 270, 21181–21187. 10.1074/jbc.270.36.21181. [PubMed: 7545666]

27. Chaudhri A, Xiao Y, Klee AN, Wang X, Zhu B, and Freeman GJ (2018). PD-L1 Binds to B7–1 Only In Cis on the Same Cell Surface. Cancer Immunology Research 6, 921–929. 10.1158/2326-6066.Cir-17-0316. [PubMed: 29871885]

28. Zhao Y, Lee CK, Lin C-H, Gassen RB, Xu X, Huang Z, Xiao C, Bonorino C, Lu L-F, and Bui JD (2019). PD-L1:CD80 cis-heterodimer triggers the co-stimulatory receptor CD28 while repressing the inhibitory PD-1 and CTLA-4 pathways. Immunity 51, 1059–1073. e1059. 10.1016/j.immuni.2019.11.003. [PubMed: 31757674]

29. Sugiura D, Maruhashi T, Okazaki I. m., Shimizu K, Maeda TK, Takemoto T, and Okazaki T (2019). Restriction of PD-1 function by cis-PD-L1/CD80 interactions is required for optimal T cell responses. Science 364, 558–566. 10.1126/science.aav7062. [PubMed: 31000591]

30. Bodle CR, Hayes MP, O'Brien JB, and Roman DL (2017). Development of a bimolecular luminescence complementation assay for RGS: G protein interactions in cells. Analytical Biochemistry 522, 10–17. 10.1016/j.ab.2017.01.013. [PubMed: 28115169]

31. Jones T, Liu A, and Cui B (2020). Light-Inducible Generation of Membrane Curvature in Live Cells with Engineered BAR Domain Proteins. ACS Synthetic Biology 9, 893–901. 10.1021/acssynbio.9b00516. [PubMed: 32212723]

32. Badour K, McGavin MKH, Zhang J, Freeman S, Vieira C, Filipp D, Julius M, Mills GB, and Siminovitch KA (2007). Interaction of the Wiskott-Aldrich syndrome protein with sorting nexin 9 is required for CD28 endocytosis and cosignaling in T cells. Proceedings of the National Academy of Sciences of the United States of America 104, 1593–1598. 10.1073/pnas.0610543104. [PubMed: 17242350]

33. Benmerah A, Bayrou M, Cerf-Bensussan N, and Dautry-Varsat A (1999). Inhibition of clathrin-coated pit assembly by an Eps15 mutant. Journal of Cell Science 112, 1303–1311. 10.1242/jcs.112.9.1303. [PubMed: 10194409]

34. Céfaï D, Schneider H, Matangkasombut O, Kang H, Brody J, and Rudd CE (1998). CD28 Receptor Endocytosis Is Targeted by Mutations That Disrupt Phosphatidylinositol 3-Kinase Binding and Costimulation. The Journal of Immunology 160, 2223–2230.doi.org/10.4049/jimmunol.160.5.2223. [PubMed: 9498761]

35. Watson RT, and Pessin JE (2001). Transmembrane domain length determines intracellular membrane compartment localization of syntaxins 3, 4, and 5. American Journal of Physiology-Cell Physiology 281, C215–C223. 10.1152/ajpcell.2001.281.1.C215. [PubMed: 11401844]

36. Mercanti V, Marchetti A, Lelong E, Perez F, Orci L, and Cosson P (2010). Transmembrane domains control exclusion of membrane proteins from clathrin-coated pits. Journal of Cell Science 123, 3329–3335. 10.1242/jcs.073031. [PubMed: 20826467]

37. Dodson LF, Boomer JS, Deppong CM, Shah DD, Sim J, Bricker TL, Russell JH, and Green JM (2009). Targeted Knock-In Mice Expressing Mutations of CD28 Reveal an Essential Pathway for Costimulation. Molecular and Cellular Biology 29, 3710–3721. 10.1128/mcb.01869-08. [PubMed: 19398586]

38. Andres PG, Howland KC, Nirula A, Kane LP, Barron L, Dresnek D, Sadra A, Imboden J, Weiss A, and Abbas AK (2004). Distinct regions in the CD28 cytoplasmic domain are required for T helper type 2 differentiation. Nature Immunology 5, 435–442. 10.1038/ni1044. [PubMed: 15004555]

39. Han Y, Branon TC, Martell JD, Boassa D, Shechner D, Ellisman MH, and Ting A (2019). Directed Evolution of Split APEX2 Peroxidase. ACS Chemical Biology 14, 619–635. 10.1021/acschembio.8b00919. [PubMed: 30848125]

40. Götzke H, Kilisch M, Martínez-Carranza M, Sograte-Idrissi S, Rajavel A, Schlichthaerle T, Engels N, Jungmann R, Stenmark P, Opazo F, and Frey S (2019). The ALFA-tag is a highly versatile tool for nanobody-based bioscience applications. Nature Communications 10, 4403. 10.1038/s41467-019-12301-7.

41. Yokosuka T, Kobayashi W, Sakata-Sogawa K, Takamatsu M, Hashimoto-Tane A, Dustin ML, Tokunaga M, and Saito T (2008). Spatiotemporal regulation of T cell costimulation by TCR-CD28 microclusters and protein kinase C theta translocation. Immunity 29, 589–601. 10.1016/j.immuni.2008.08.011. [PubMed: 18848472]

42. Tseng S-Y, Waite JC, Liu M, Vardhana S, and Dustin ML (2008). T cell-dendritic cell immunological synapses contain TCR-dependent CD28-CD80 clusters that recruit protein kinase C theta. Journal of immunology (Baltimore, Md. : 1950) 181, 4852–4863. 10.4049/jimmunol.181.7.4852. [PubMed: 18802089]

43. Coudronniere N, Villalba M, Englund N, and Altman A (2000). NF-kappa B activation induced by T cell receptor/CD28 costimulation is mediated by protein kinase C-theta. Proceedings of the National Academy of Sciences of the United States of America 97, 3394–3399. 10.1073/pnas.97.7.3394. [PubMed: 10716728]

44. Griffiths GM, Tsun A, and Stinchcombe JC (2010). The immunological synapse: a focal point for endocytosis and exocytosis. Journal of Cell Biology 189, 399–406. 10.1083/jcb.201002027. [PubMed: 20439993]

45. Onnis A, and Baldari CT (2019). Orchestration of Immunological Synapse Assembly by Vesicular Trafficking. Frontiers in Cell and Developmental Biology 7. 10.3389/fcell.2019.00110.

46. Hofinger E, and Sticht H (2005). Multiple modes of interaction between Lck and CD28. J Immunol 174, 3839–3840; author reply 3840. 10.4049/jimmunol.174.7.3839-a.

47. Dobbins J, Gagnon E, Godec J, Pyrdol J, Vignali DAA, Sharpe AH, and Wucherpfennig KW (2016). Binding of the cytoplasmic domain of CD28 to the plasma membrane inhibits Lck recruitment and signaling. Science signaling 9, ra75–ra75. 10.1126/scisignal.aaf0626. [PubMed: 27460989]

48. Yang W, Pan W, Chen S, Trendel N, Jiang S, Xiao F, Xue M, Wu W, Peng Z, Li X, et al. (2017). Dynamic regulation of CD28 conformation and signaling by charged lipids and ions. Nature Structural & Molecular Biology 24, 1081–1092. 10.1038/nsmb.3489.

49. Ecker M, Schregle R, Kapoor-Kaushik N, Rossatti P, Betzler VM, Kempe D, Biro M, Ariotti N, Redpath GMI, and Rossy J (2022). SNX9-induced membrane tubulation regulates CD28 cluster stability and signalling. eLife 11, e67550. 10.7554/eLife.67550. [PubMed: 35050850]

50. Feng Z, and Yu C. h. (2021). PI(3,4)P2-mediated membrane tubulation promotes integrin trafficking and invasive cell migration. Proceedings of the National Academy of Sciences 118, e2017645118. doi:10.1073/pnas.2017645118.

51. Burr JS, Savage NDL, Messah GE, Kimzey SL, Shaw AS, Arch RH, and Green JM (2001). Cutting Edge: Distinct Motifs Within CD28 Regulate T Cell Proliferation and Induction of Bcl-XL. The Journal of Immunology 166, 5331–5335. 10.4049/jimmunol.166.9.5331. [PubMed: 11313368]

52. Okkenhaug K, Wu L, Garza KM, La Rose J, Khoo W, Odermatt B, Mak TW, Ohashi PS, and Rottapel R (2001). A point mutation in CD28 distinguishes proliferative signals from survival signals. Nature Immunology 2, 325–332. 10.1038/86327. [PubMed: 11276203]

53. Mirenda V, Jarmin SJ, David R, Dyson J, Scott D, Gu Y, Lechler RI, Okkenhaug K, and Marelli-Berg FM (2006). Physiologic and aberrant regulation of memory T-cell trafficking by the costimulatory molecule CD28. Blood 109, 2968–2977. 10.1182/blood-2006-10-050724.

54. Chong H, Hutchinson G, Hart IR, and Vile RG (1998). Expression of B7 co-stimulatory molecules by B16 melanoma results in a natural killer cell-dependent local anti-tumour response, but induces T-cell-dependent systemic immunity only against B7-expressing tumours. Br J Cancer 78, 1043–1050. 10.1038/bjc.1998.625. [PubMed: 9792148]

55. van der Windt GJ, Everts B, Chang C-H, Curtis JD, Freitas TC, Amiel E, Pearce EJ, and Pearce EL (2012). Mitochondrial respiratory capacity is a critical regulator of CD8+ T cell memory development. Immunity 36, 68–78. 10.1016/j.immuni.2011.12.007. [PubMed: 22206904]

56. Chan PY, and Aruffo A (1993). VLA-4 integrin mediates lymphocyte migration on the inducible endothelial cell ligand VCAM-1 and the extracellular matrix ligand fibronectin. Journal of Biological Chemistry 268, 24655–24664. 10.1016/S0021-9258(19)74516-5. [PubMed: 7693704]

57. Krummel MF, Bartumeus F, and Gérard A (2016). T cell migration, search strategies and mechanisms. Nature Reviews Immunology 16, 193–201. 10.1038/nri.2015.16.

58. Walling BL, and Kim M (2018). LFA-1 in T Cell Migration and Differentiation. Frontiers in Immunology 9. 10.3389/fimmu.2018.00952.

59. Wyss-Coray T, Mauri-Hellweg D, Baumann K, Bettens F, Grunow R, and Pichler WJ (1993). The B7 adhesion molecule is expressed on activated human T cells: Functional involvement in T-T cell interactions. European Journal of Immunology 23, 2175–2180. 10.1002/eji.1830230919. [PubMed: 7690323]

60. Broz Miranda L., Binnewies M, Boldajipour B, Nelson Amanda E., Pollack Joshua L., Erle David J., Barczak A, Rosenblum Michael D., Daud A, Barber Diane L., et al. (2014). Dissecting the Tumor Myeloid Compartment Reveals Rare Activating Antigen-Presenting Cells Critical for T Cell Immunity. Cancer Cell 26, 638–652. 10.1016/j.ccell.2014.09.007. [PubMed: 25446897]

61. Gerhard GM, Bill R, Messemaker M, Klein AM, and Pittet MJ (2021). Tumor-infiltrating dendritic cell states are conserved across solid human cancers. J Exp Med 218, e20200264. 10.1084/jem.20200264. [PubMed: 33601412]

62. Murphy TL, and Murphy KM (2022). Dendritic cells in cancer immunology. Cell Mol Immunol 19, 3–13. 10.1038/s41423-021-00741-5. [PubMed: 34480145]

63. Roberts EW, Broz ML, Binnewies M, Headley MB, Nelson AE, Wolf DM, Kaisho T, Bogunovic D, Bhardwaj N, and Krummel MF (2016). Critical Role for CD103+/CD141+ Dendritic Cells Bearing CCR7 for Tumor Antigen Trafficking and Priming of T Cell Immunity in Melanoma. Cancer Cell 30, 324–336. 10.1016/j.ccell.2016.06.003. [PubMed: 27424807]

64. Wang C, Lin GH, McPherson AJ, and Watts TH (2009). Immune regulation by 4–1BB and 4–1BBL: complexities and challenges. Immunol Rev 229, 192–215. 10.1111/j.1600-065X.2009.00765.x. [PubMed: 19426223]

65. Croft M (2009). The role of TNF superfamily members in T-cell function and diseases. Nat Rev Immunol 9, 271–285. 10.1038/nri2526. [PubMed: 19319144]

66. Zenke S, Palm MM, Braun J, Gavrilov A, Meiser P, Böttcher JP, Beyersdorf N, Ehl S, Gerard A, Lämmermann T, et al. (2020). Quorum Regulation via Nested Antagonistic Feedback

Circuits Mediated by the Receptors CD28 and CTLA-4 Confers Robustness to T Cell Population Dynamics. Immunity 52, 313–327.e317. 10.1016/j.immuni.2020.01.018. [PubMed: 32049052]

67. Hommel M, and Kyewski B (2003). Dynamic changes during the immune response in T cell-antigen-presenting cell clusters isolated from lymph nodes. J Exp Med 197, 269–280. 10.1084/jem.20021512. [PubMed: 12566411]

68. Salazar-Fontana LI, Barr V, Samelson LE, and Bierer BE (2003). CD28 engagement promotes actin polymerization through the activation of the small Rho GTPase Cdc42 in human T cells. The Journal of Immunology 171, 2225–2232. 10.4049/jimmunol.171.5.2225. [PubMed: 12928366]

69. Sorkin A, and von Zastrow M (2009). Endocytosis and signalling: intertwining molecular networks. Nature Reviews Molecular Cell Biology 10, 609–622. 10.1038/nrm2748. [PubMed: 19696798]

70. Harada Y, Tokushima M, Matsumoto Y, Ogawa S, Otsuka M, Hayashi K, Weiss BD, June CH, and Abe R (2001). Critical Requirement for the Membrane-Proximal Cytosolic Tyrosine Residue for CD28-Mediated Costimulation In Vivo. The Journal of Immunology 166, 3797–3803. 10.4049/jimmunol.166.6.3797. [PubMed: 11238622]

71. Boomer JS, Deppong CM, Shah DD, Bricker TL, and Green JM (2014). Cutting Edge: A Double-Mutant Knockin of the CD28 YMNM and PYAP Motifs Reveals a Critical Role for the YMNM Motif in Regulation of T Cell Proliferation and Bcl-xL Expression. The Journal of Immunology 192, 3465–3469. 10.4049/jimmunol.1301240. [PubMed: 24639356]

72. Okkenhaug K, Ali K, and Vanhaesebroeck B (2007). Antigen receptor signalling: a distinctive role for the p110δ isoform of PI3K. Trends Immunol 28, 80–87. 10.1016/j.it.2006.12.007. [PubMed: 17208518]

73. Kin NW, and Sanders VM (2006). CD86 stimulation on a B cell activates the phosphatidylinositol 3-kinase/Akt and phospholipase C gamma 2/protein kinase C alpha beta signaling pathways. J Immunol 176, 6727–6735. 10.4049/jimmunol.176.11.6727. [PubMed: 16709832]

74. Li B, Lu Y, Zhong M-C, Qian J, Li R, Davidson D, Tang Z, Zhu K, Argenty J, de Peredo AG, et al. (2022). Cis interactions between CD2 and its ligands on T cells are required for T cell activation. Science Immunology 7, eabn6373. doi:10.1126/sciimmunol.abn6373. [PubMed: 35930657]

75. McArdel SL, Terhorst C, and Sharpe AH (2016). Roles of CD48 in regulating immunity and tolerance. Clinical immunology 164, 10–20. 10.1016/j.clim.2016.01.008. [PubMed: 26794910]

76. Muhammad A, Schiller HB, Forster F, Eckerstorfer P, Geyeregger R, Leksa V, Zlabinger GJ, Sibilia M, Sonnleitner A, Paster W, and Stockinger H (2009). Sequential Cooperation of CD2 and CD48 in the Buildup of the Early TCR Signalosome. The Journal of Immunology 182, 7672–7680. 10.4049/jimmunol.0800691. [PubMed: 19494291]

77. Pielak RM, O'Donoghue GP, Lin JJ, Alfieri KN, Fay NC, Low-Nam ST, and Groves JT (2017). Early T cell receptor signals globally modulate ligand:receptor affinities during antigen discrimination. Proceedings of the National Academy of Sciences 114, 12190–12195. doi:10.1073/pnas.1613140114.

78. Pylypenko O, Lundmark R, Rasmuson E, Carlsson SR, and Rak A (2007). The PX-BAR membrane-remodeling unit of sorting nexin 9. EMBO J 26, 4788–4800. 10.1038/sj.emboj.7601889. [PubMed: 17948057]

79. van Weering JR, Sessions RB, Traer CJ, Kloer DP, Bhatia VK, Stamou D, Carlsson SR, Hurley JH, and Cullen PJ (2012). Molecular basis for SNX-BAR-mediated assembly of distinct endosomal sorting tubules. EMBO J 31, 4466–4480. 10.1038/emboj.2012.283. [PubMed: 23085988]

80. Soulet F, Yarar D, Leonard M, and Schmid SL (2005). SNX9 regulates dynamin assembly and is required for efficient clathrin-mediated endocytosis. Mol Biol Cell 16, 2058–2067. 10.1091/mbc.e04-11-1016. [PubMed: 15703209]

81. Orbach R, and Su X (2020). Surfing on Membrane Waves: Microvilli, Curved Membranes, and Immune Signaling. Front Immunol 11, 2187. 10.3389/fimmu.2020.02187. [PubMed: 33013920]

82. Cai E, Marchuk K, Beemiller P, Beppler C, Rubashkin MG, Weaver VM, Gérard A, Liu TL, Chen BC, Betzig E, et al. (2017). Visualizing dynamic microvillar search and stabilization during ligand detection by T cells. Science 356. 10.1126/science.aal3118.

83. Fairhead M, and Howarth M (2015). Site-specific biotinylation of purified proteins using BirA. Methods in molecular biology (Clifton, N.J.) 1266, 171–184. 10.1007/978-1-4939-2272-7_12.

84. Xia Z, and Liu Y (2001). Reliable and global measurement of fluorescence resonance energy transfer using fluorescence microscopes. Biophysical journal 81, 2395–2402. 10.1016/S0006-3495(01)75886-9. [PubMed: 11566809]

85. Roszik J, Szöll si J, and Vereb G (2008). AccPbFRET: An ImageJ plugin for semi-automatic, fully corrected analysis of acceptor photobleaching FRET images. BMC Bioinformatics 9, 346. 10.1186/1471-2105-9-346. [PubMed: 18713453]

86. Ovesný M, K ížek P, Borkovec J, Švindrych Z, and Hagen GM (2014). ThunderSTORM: a comprehensive ImageJ plug-in for PALM and STORM data analysis and super-resolution imaging. Bioinformatics 30, 2389–2390. 10.1093/bioinformatics/btu202. [PubMed: 24771516]

87. Levet F, Julien G, Galland R, Butler C, Beghin A, Chazeau A, Hoess P, Ries J, Giannone G, and Sibarita J-B (2019). A tessellation-based colocalization analysis approach for single-molecule localization microscopy. Nature Communications 10, 2379. 10.1038/s41467-019-10007-4.

88. Desta IT, Porter KA, Xia B, Kozakov D, and Vajda S (2020). Performance and Its Limits in Rigid Body Protein-Protein Docking. Structure 28, 1071–1081.e1073. 10.1016/j.str.2020.06.006. [PubMed: 32649857]

89. Vajda S, Yueh C, Beglov D, Bohnuud T, Mottarella SE, Xia B, Hall DR, and Kozakov D (2017). New additions to the ClusPro server motivated by CAPRI. Proteins 85, 435–444. 10.1002/prot.25219. [PubMed: 27936493]

90. Kozakov D, Hall DR, Xia B, Porter KA, Padhorny D, Yueh C, Beglov D, and Vajda S (2017). The ClusPro web server for protein–protein docking. Nature Protocols 12, 255–278. 10.1038/nprot.2016.169. [PubMed: 28079879]

91. Kozakov D, Beglov D, Bohnuud T, Mottarella SE, Xia B, Hall DR, and Vajda S (2013). How good is automated protein docking? Proteins 81, 2159–2166. 10.1002/prot.24403. [PubMed: 23996272]

92. Stamper CC, Zhang Y, Tobin JF, Erbe DV, Ikemizu S, Davis SJ, Stahl ML, Seehra J, Somers WS, and Mosyak L (2001). Crystal structure of the B7–1/CTLA-4 complex that inhibits human immune responses. Nature 410, 608–611. 10.1038/35069118. [PubMed: 11279502]

93. Schwartz J-CD, Zhang X, Fedorov AA, Nathenson SG, and Almo SC (2001). Structural basis for co-stimulation by the human CTLA-4/B7–2 complex. Nature 410, 604–608. 10.1038/35069112. [PubMed: 11279501]

94. Jumper J, Evans R, Pritzel A, Green T, Figurnov M, Ronneberger O, Tunyasuvunakool K, Bates R, Žídek A, Potapenko A, et al. (2021). Highly accurate protein structure prediction with AlphaFold. Nature 596, 583–589. 10.1038/s41586-021-03819-2. [PubMed: 34265844]

95. Xu X, Masubuchi T, Cai Q, Zhao Y, and Hui E (2021). Molecular features underlying differential SHP1/SHP2 binding of immune checkpoint receptors. eLife 10, e74276. 10.7554/eLife.74276. [PubMed: 34734802]

96. Zhao Y, Harrison DL, Song Y, Ji J, Huang J, and Hui E (2018). Antigen-presenting cell-intrinsic PD-1 neutralizes PD-L1 in cis to attenuate PD-1 signaling in T cells. Cell reports 24, 379–390. e376. 10.1016/j.celrep.2018.06.054. [PubMed: 29996099]

Highlights:

T cell B7 molecules bind to CD28 in *cis* at concave membranes during CD28 endocytosis

Cis-B7:CD28 interactions trigger CD28 signaling through PKCθ

CD28 *cis*-signaling is promoted by PI3K-SNX9-driven invagination of synaptic membranes

Cis-B7:CD28 signaling enhances anti-tumor response of primed CD8^{+} T cells
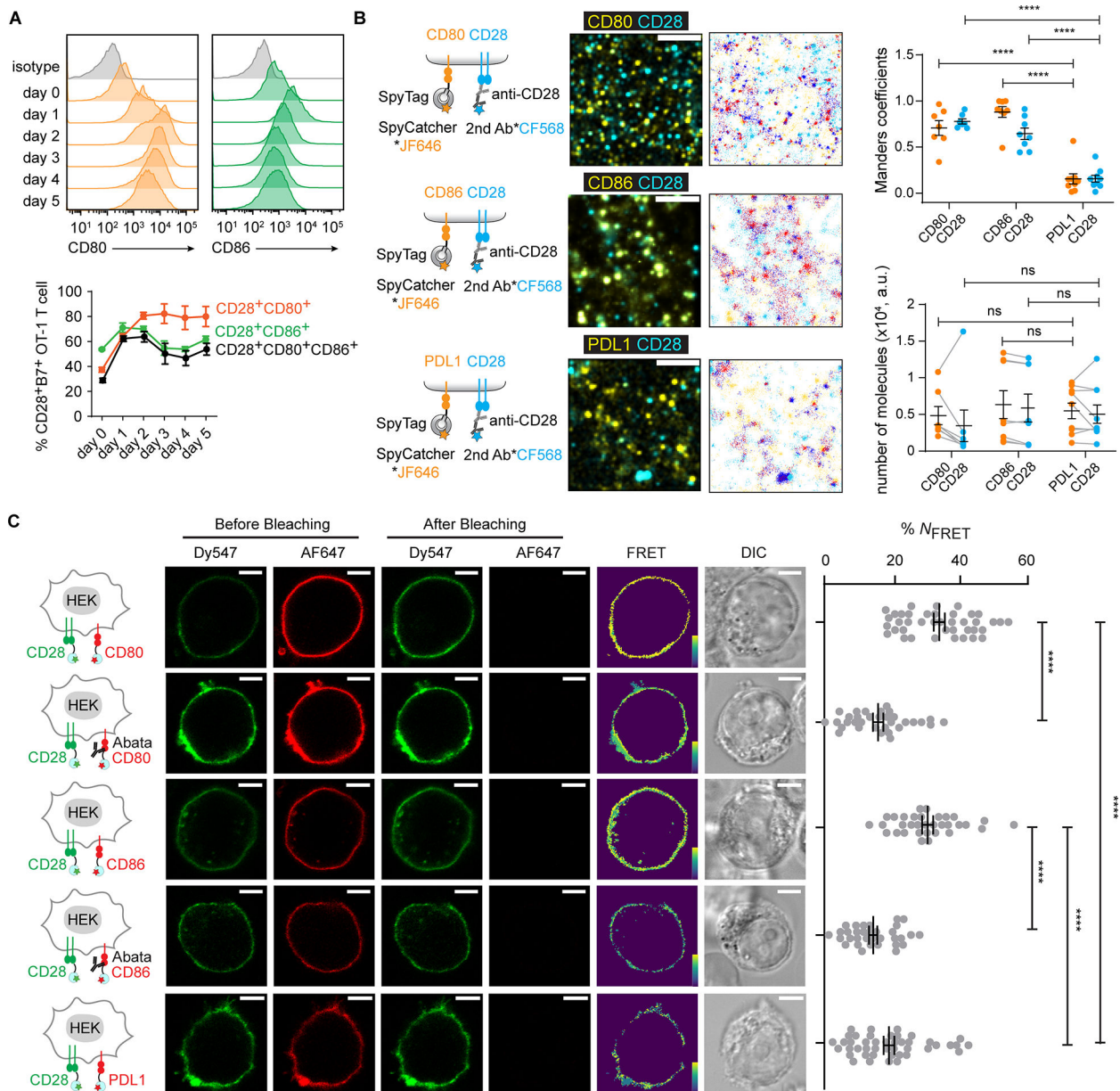
Figure 1. CD28 and B7 are co-expressed on CD8⁺ T cells, colocalize on plasma membranes, and interact in *cis*.

A) Flow cytometry histograms showing expression of CD80 and CD86 in OT-1 T cells during in *vitro* priming using OVA$_{257-264}$. The line plot shows the percentages of CD28⁺CD80⁺, CD28⁺CD86⁺, and CD28⁺CD80⁺CD86⁺ OT-1 T cells during priming. Mean ± SEM from three OT-1 mice.

(B) STORM of CD28 and Spy-CD80, CD28 and Spy-CD86, or CD28 and Spy-PDL1 on the plasma membranes of HEK293T cells. Leftmost cartoons depict the experimental scheme: CD28 stained with anti-CD28 1st antibody (Ab) and CF568-labeled 2nd Ab; SpyTagged proteins stained with JF646-labeled SpyCatcher. 2nd column: raw two-color STORM images of indicated proteins. Bars = 1 μm. 3rd column: point rendering for two-color localizations computed by Coloc-Tesseler. Blue: CD28 colocalized with B7 or PDL1. Cyan: CD28 not

colocalized with B7 or PDL1. Red: B7 or PDL1 colocalized with CD28. Yellow: B7 or PDL1 not colocalized with CD28. Upper dot plot: Manders coefficients calculated using CD28 as a reference (orange) or using CD80, CD86, or PDL1 as a reference (cyan), based on 2–3 random $3 \times 3 \ \mu m^2$ areas from each cell, n 6 areas from three independent experiments. Lower dot plot: number of molecules counted from each area, grey lines connect data points within the same areas.

(C) FRET data of *cis*-B7:CD28 interactions. Leftmost cartoons show cells co-expressing CLIP-CD28 (Dy547 labeled) and SNAP-tagged CD80, CD86, or PDL1 (AF647 labeled), ± abatacept (Abata). Columns 2–5: confocal images of Dy547 and AF647 channels before and after AF647 photobleaching. Bar = 5 μm. Column 6: calculated pseudo-color FRET efficiency image (yellow to violet denotes strong to weak FRET). Column 7: DIC image. Dot plot: FRET efficiencies (N_{FRET}) from n > 33 cells in three independent experiments. Mean ± SEM. One-way ANOVA: ****p < 0.0001. See also Figure S1.
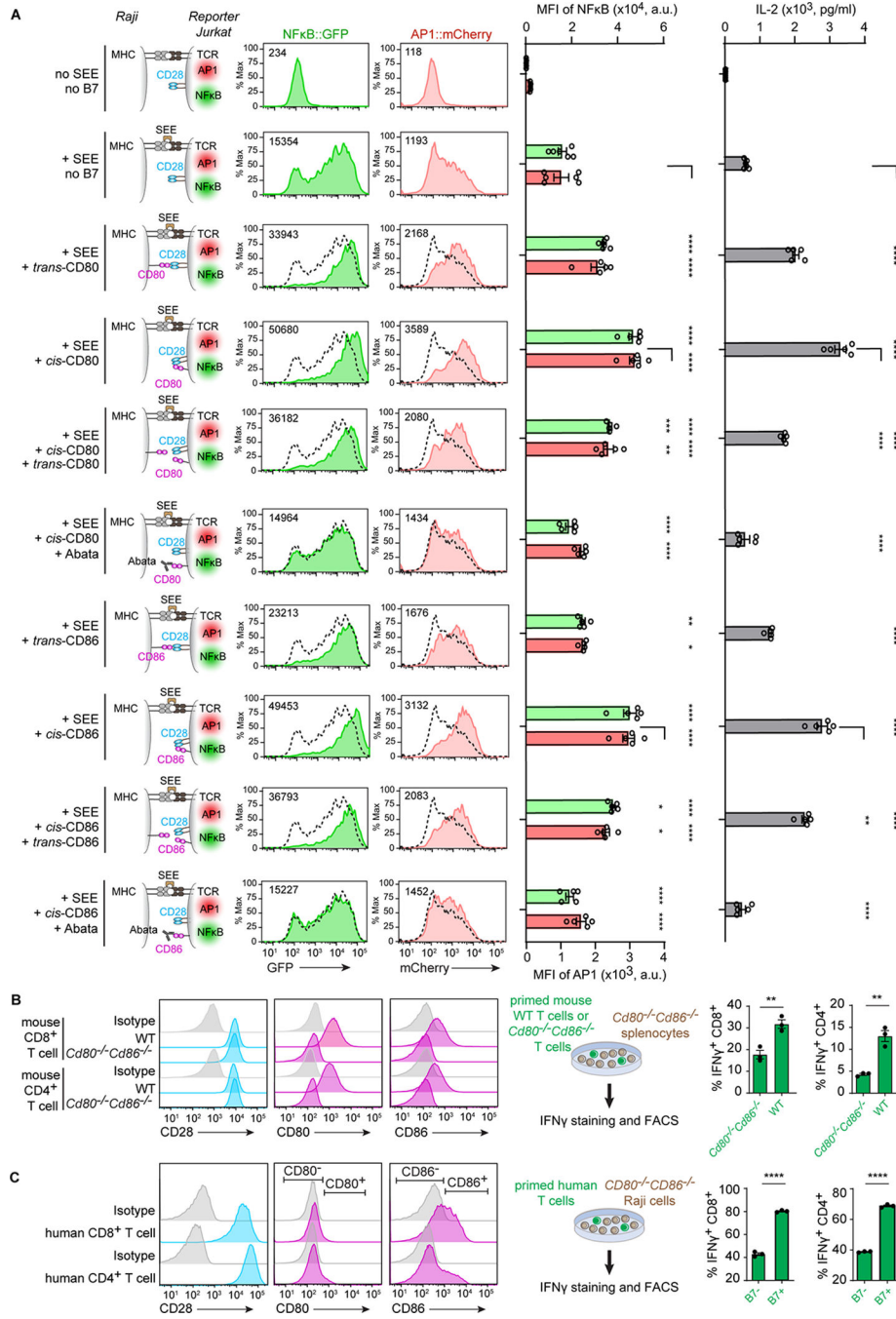
Figure 2. *Cis*-B7:CD28 interactions promote NFκB, AP1, IL-2, and IFNγ expression in T cells.
(**A**) Cartoons on the left depict *CD28^{+/+}NFκB:GFP^+AP1:mCherry^+* reporter Jurkat cell cocultured with Raji APCs, with CD80 or CD86 expressed on either Jurkat cell (*cis*) or Raji cell (*trans*), ± Abatacept. Flow cytometry histograms show GFP and mCherry expression with the mean fluorescence intensity (MFI) indicated. Histograms in condition 2 are shown as dashed lines in conditions 3–10 as references. Green and red bars summarize GFP (NFκB) and mCherry (AP1) MFI respectively. Bar graph: IL-2 concentration in media after 16 h coculture. Data obtained from 5 independent experiments.

(**B**) Left, CD28, CD80 and CD86 expression on primed mouse T cells. Right, scheme of primed T cells cocultured with anti-CD3ε-loaded splenocytes. Bar graph: % IFNγ+ T cells after 6 h coculture. Data obtained from 3 independent experiments.

(**C**) Left, CD28, CD80 and CD86 expression on primed human T cells and gating strategy. Right, scheme of primed T cells cocultured with SEB-loaded Raji cell. Bar graph: % IFNγ+ T cells after 6 h coculture. Data obtained from 3 technical replicates using T cells from one donor.

Data shown as mean ± SEM. One-way ANOVA (A) and unpaired two-tailed Student's t test (B, C): *p < 0.05, **p < 0.01, ***p < 0.001, ****p < 0.0001. See also Figure S2.
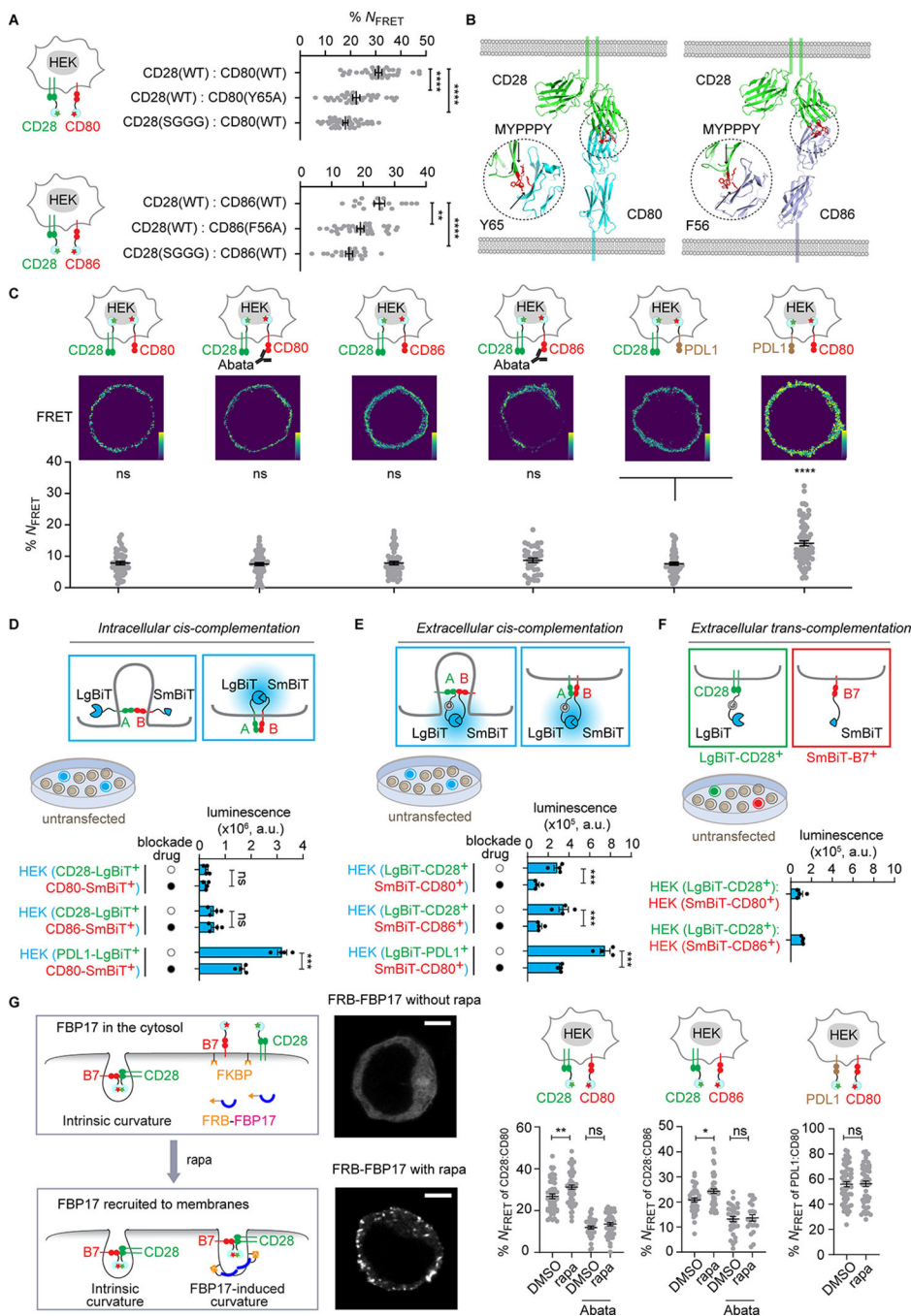
Figure 3. *Cis*-B7:CD28 interactions occur head-to-head and are promoted by negative membrane curvatures.

(A) Dot plots summarizing *cis*-CD80:CD28 FRET and *cis*-CD86:CD28 FRET when indicated CD28 and B7 were co-expressed in HEK293T cells. Fluorophores coupled to ECDs as in Figure 1C. n > 20 cells from three independent experiments.

(B) Ribbon diagrams of predicted CD80:CD28 and CD86:CD28 structures. Dash circles: indicate B7:CD28 binding interfaces. Red residues crucial for interactions.

(C) FRET efficiency images and dot plots summarizing *cis*-CD28:B7 FRET, *cis*-CD28:PDL1 FRET, and *cis*-PDL1:CD80 FRET, when the indicated protein pairs were co-expressed in HEK293T cells, with the fluorophores coupled to their ICDs, indicated in the cartoons. n > 36 cells from 3 independent experiments.

(D) A BiLC assay probing the CD28-ICD:B7-ICD proximity with LgBiT and SmBiT fused to the C-terminus of ICDs. Cartoon depicts the theoretical outcomes of head-to-head versus side-by-side binding. Low transfection efficiency allowed untransfected cells to serve as filler cells, limiting *trans*-contact of double positive cells. Positive control: PDL1:CD80 pair. Bar graphs show luminescence intensity ± blockade drug (Abatacept for *cis*-B7:CD28, atezolizumab for *cis*-CD80:PDL1).

(E) Same as D except that LgBiT and SmBiT were coupled to the N-terminus of ECDs, to probe ECD proximity within a *cis*-complex. Cartoon depicts the theoretical outcomes. Bar graph summarizes the experimental data.

(F) Control experiments showing limited *trans*-B7:CD28 interactions due to excess filler cells. LgBiT-CD28 singly-transfected cells incubated with SmBiT-B7 singly-transfected cells in the presence of excess untransfected filler cells. Luminescence data summarized in the bar graph as mean ± SEM from four independent experiments.

(E) Effects of FBP17-induced membrane curvatures on *cis*-B7:CD28 FRET. HEK293T cells expressed CLIP-CD28, SNAP-B7, FKBP-TagBFP-CAAX, and mGFP-FRB-FBP17. Cartoon depicts a likely series of molecular events: Rapa induces membrane recruitment mGFP-FRB-FBP17, which invaginates the membranes to promote *cis*-CD28:B7 interactions. Confocal images show Rapa effects on mGFP-FRB-FBP17 localizations. Dot plot summarizes *cis*-B7:CD28 and *cis*-CD80:PDL1 FRET of HEK293T cells treated with DMSO or Rapa, ± Abata from n > 21 cells from 3 independent experiments.

Unpaired two-tailed Student's t test (D, E) and One-way ANOVA (B-F): *p < 0.05, **p < 0.01, ***p < 0.001, ****p < 0.0001. See also Figure S3.
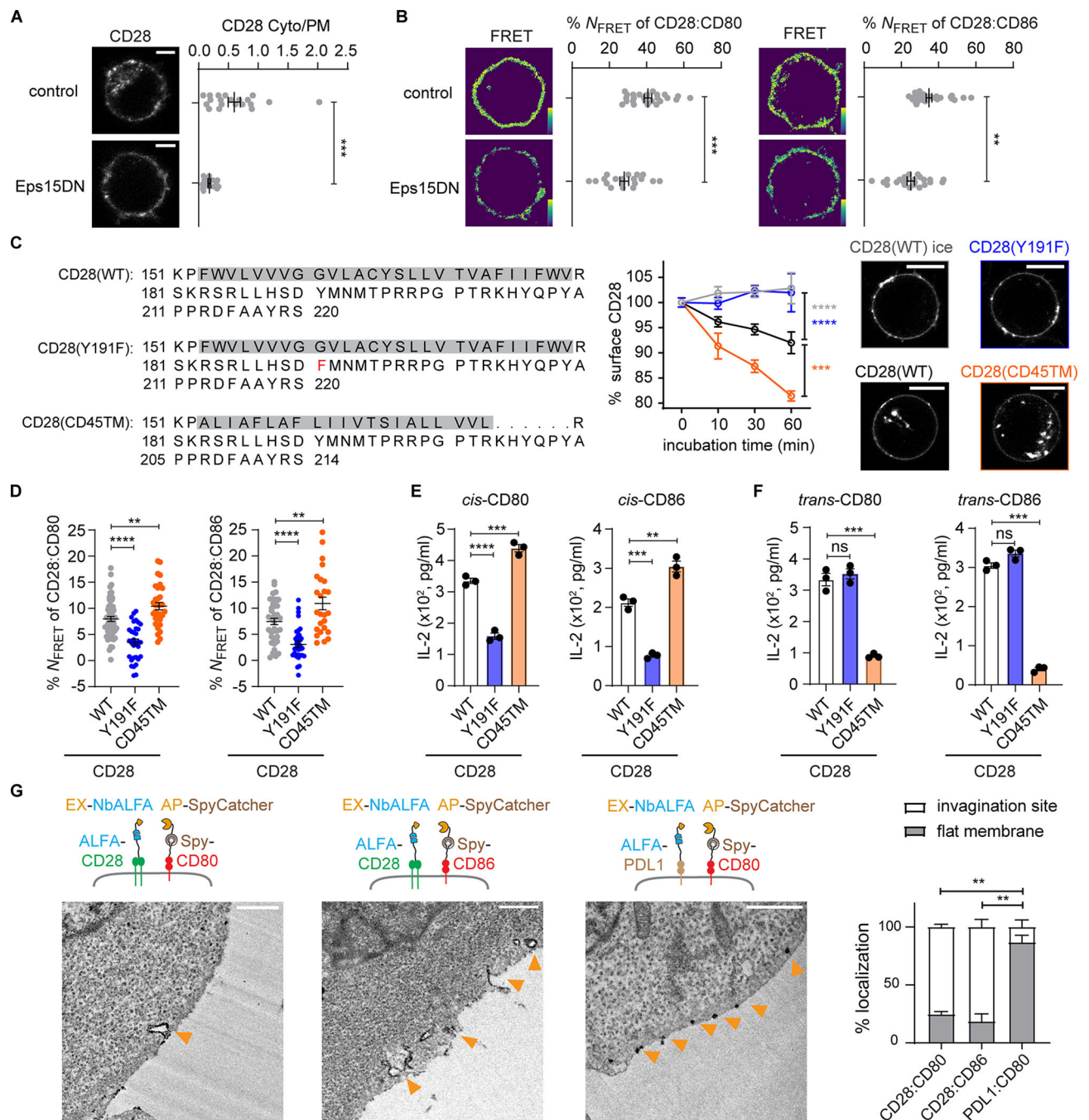
Figure 4. Cis-B7:CD28 interactions depend on CD28 endocytosis.

(A) Effects of Eps15DN on *cis*-B7:CD28 interactions. Left, confocal images of Dy547*CLIP-CD28 expressed in HEK293T cells with or without co-transfection with Eps15DN. Dot plot: ratio of intracellular CD28 to cell surface CD28 of n > 16 cells from three independent experiments.

(B) Left, Dy547*CLIP-CD28:AF647*SNAP-CD80 FRET in HEK293T cells (control) and HEK293T cells co-transfected with Eps15DN. Dot plot: N_{FRET} of n > 20 cells from three

independent experiments. Right, same as Left except replacing CD80 with CD86, n > 23 cells from three independent experiments. Bar = 5 μm.

(C) Internalization kinetics of CD28 mutants. Jurkat cells transduced with Spy-CD28, Spy-CD28(Y191F), or Spy-CD28(CD45TM), with amino acid (AA) sequence of TMD and ICD shown, were labeled with biotinylated SpyCatcher on ice, followed by incubation at 37 °C or on ice. Cell surface CD28 stained by AF647-conjugated streptavidin, measured by flow cytometry, normalized to AF647 MFI at 0 min, and plotted against time (mean ± SEM, n > 5). Confocal images of indicated Jurkat cell taken after 60 min incubation at 37 °C upon staining Spy-CD28 proteins with JF646*SpyCatcher. Bar = 10 μm.

(D) Dot plots summarizing the FRET between indicated CLIP-CD28 variants and SNAP-B7. n > 24 cells in 3 independent experiments.

(E) Effects of CD28 endocytosis mutants on *cis*-B7 induced IL-2 secretion. Jurkat co-expressing CD28(WT) or indicated mutant with CD80 or CD86 cocultured with excess SEE-loaded *CD80$^{-/-}$CD86$^{-/-}$* Raji APCs. Bar graphs summarize IL-2 in the media in three independent experiments.

(F) Effects of CD28 endocytosis mutants on *trans*-B7 induced IL-2 secretion. Same as E except that CD80 or CD86 was expressed in Raji cell rather than in Jurkat cell.

(G) Localizing *cis*-B7:CD28 complexes and *cis*-CD80:PDL1 complexes using Split-APEX2 and TEM. Jurkat cells co-expressing ALFA-CD28 and Spy-B7, or ALFA-PDL1 and Spy-CD80 were labeled by EX-NbALFA and AP-SpyCatcher. Functional APEX2 detected by DAB staining, observed using TEM, denoted by orange arrows. Bar graph: % DAB stains on flat membrane and invaginated membrane of n > 17 cells from two independent experiments. Bar = 0.5 μm. Unpaired two-tailed Student's t test (A), One-way ANOVA (C-F) and Two-way ANOVA (B): *p < 0.05, **p < 0.01, ***p < 0.001, ****p < 0.0001. See also Figure S4.
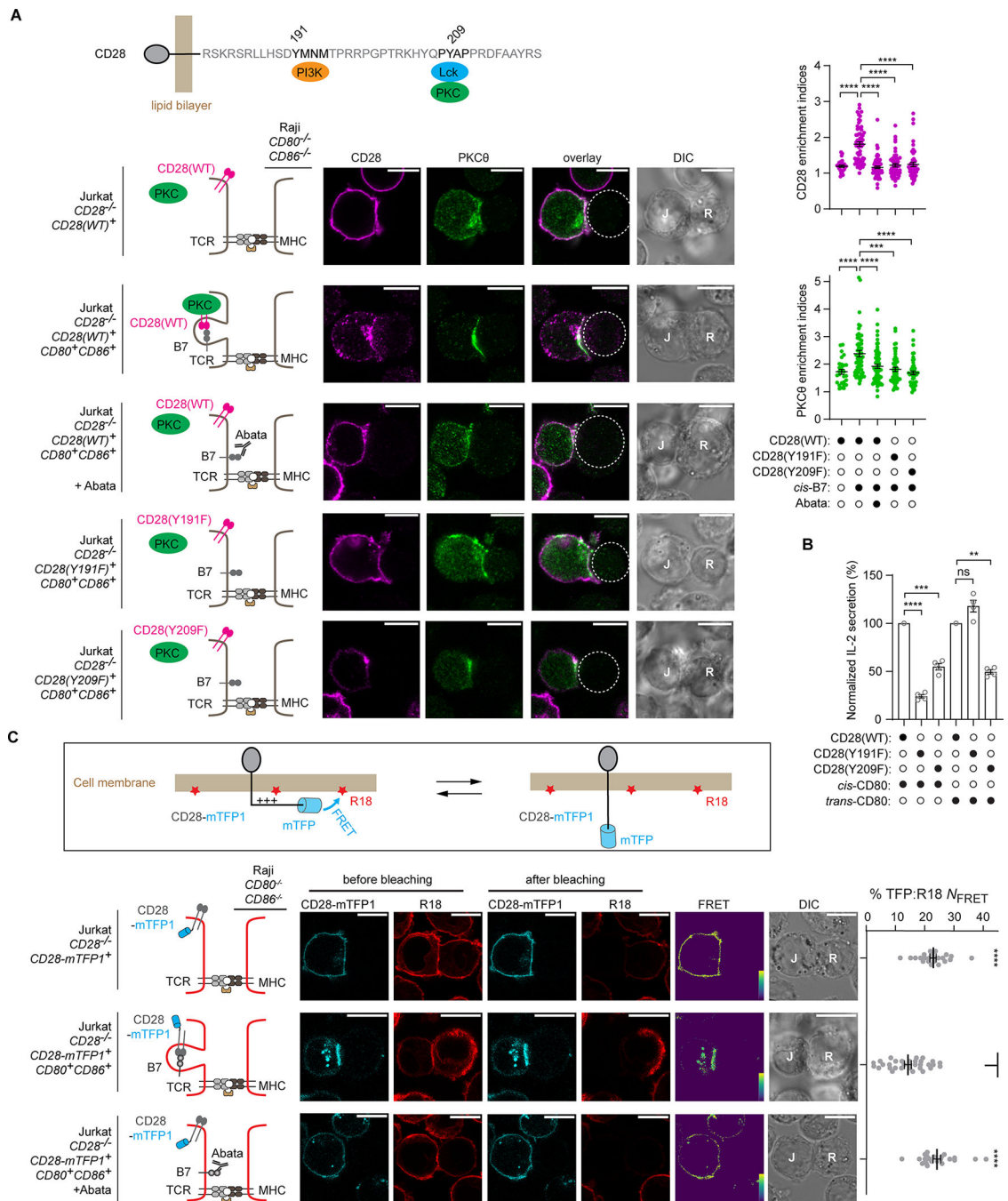
Figure 5. *Cis*-B7 promotes the synaptic enrichment of CD28 and PKCθ and decreases the membrane association of CD28 ICD.

(A) Effects of *cis*-B7 on CD28 and PKCθ localizations. Cartoon on top: AA sequence of human CD28 ICD with PI3K, Lck, and PKCθ binding motifs highlighted. Leftmost cartoons depict a $CD80^{-/-}CD86^{-/-}$ Raji cell contacting a $CD28^+$ Jurkat cell, a $CD28^+B7^+$ Jurkat cell, an Abata-treated $CD28^+B7^+$ Jurkat cell, a $CD28(Y191F)^+B7^+$ Jurkat cell or a $CD28(Y209F)^+B7^+$ Jurkat cell. Immediate right are confocal images of immunostained CD28 and PKCθ acquired 30 min after Jurkat:Raji cell contact. Dashed circles indicate Raji

cells conjugated to Jurkat cells. Dot plots: synaptic enrichment indices of CD28 (magenta) and PKCθ (green), n > 27 conjugates from three independent experiments. Bar = 10 μm.

(B) Bar graph summarizing IL-2 secretion by Jurkat cells expressing indicated CD28 variants cocultured with SEE-loaded Raji cells, with CD80 expressed either on Jurkat cell (in *cis*) or on Raji cell (in *trans*). Data from two independent experiments with two technical replicates each.

(C) A FRET assay showing effects of *cis*-B7 on CD28-ICD:membrane binding, depicted in cartoon on top. Leftmost cartoons depict a *CD80⁻/⁻CD86⁻/⁻* Raji cell contacting a *CD28-mTFP1⁺* Jurkat cell, a *CD28-mTFP1⁺B7⁺* Jurkat cell, or an Abata-treated *CD28-mTFP1⁺B7⁺* Jurkat cell. Immediate right are confocal images of CD28-mTFP1 and R18 before and after R18 photobleaching, and pseudo-color FRET efficiency images. Dot plots: N_{FRET} calculated based on the Jurkat:Raji cell contact zone from n > 23 conjugates in three independent experiments.

Data shown as mean ± SEM. One-way ANOVA: *$p < 0.05$, **$p < 0.01$, ***$p < 0.001$, ****$p < 0.0001$.
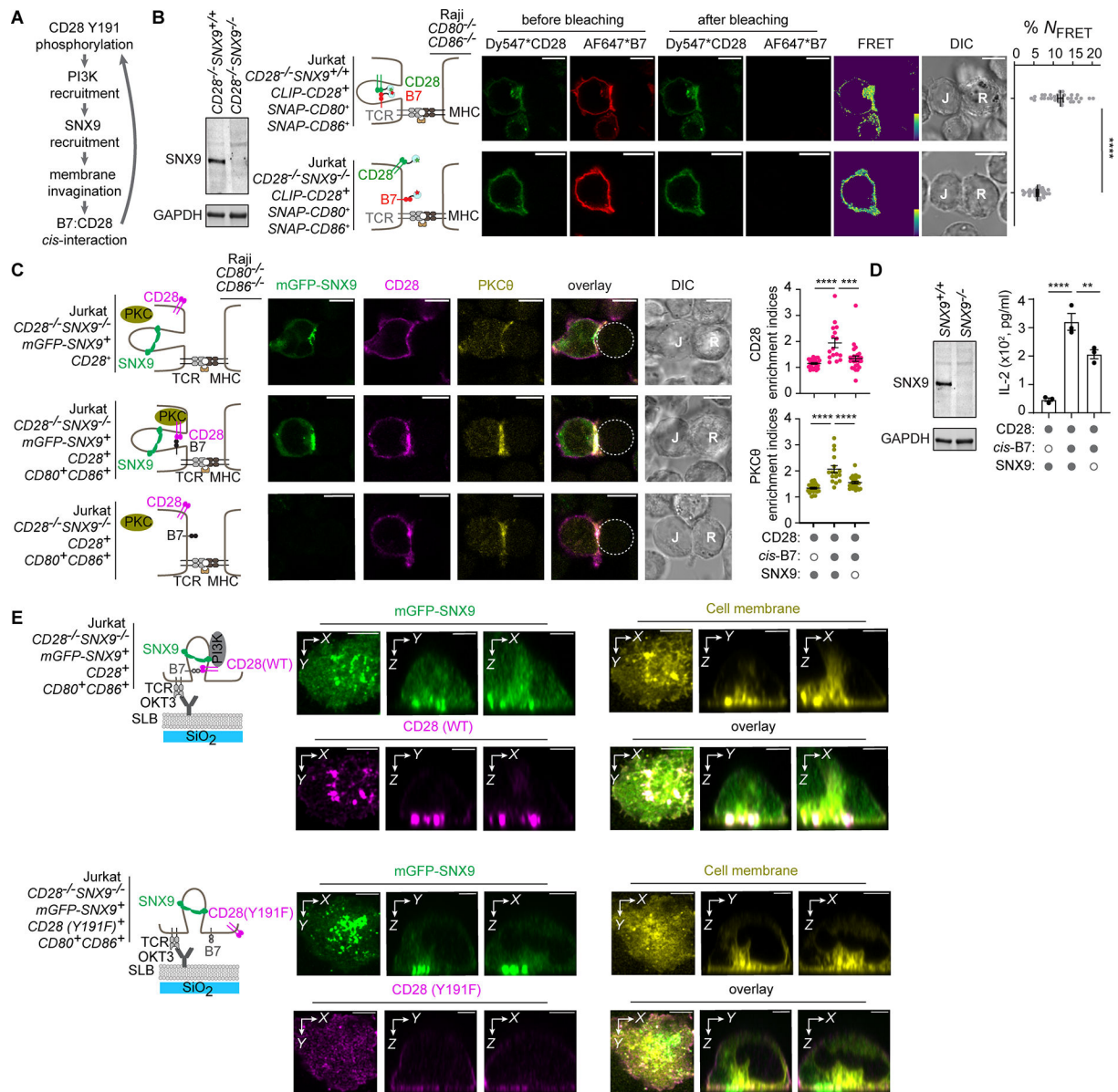
Figure 6. SNX9-induced membrane invagination at the T:APC interface promotes *cis*-B7:CD28 interactions and T cell activation.

(A) Model by which CD28:PI3K interaction promotes *cis*-B7:CD28 interactions via SNX9-driven membrane invagination.

(B) A FRET assay showing effects of SNX9 deficiency on *cis*-B7:CD28 interactions. Leftmost western blot shows SNX9 and GAPDH expression in indicated Jurkat cells. Immediate right are cartoons showing indicated Jurkat cells conjugated with $CD80^{-/-}CD86^{-/-}$ Raji cell. Further right are confocal images of Dy547 and AF647 channels before and after AF647 photobleaching, FRET efficiency image, and DIC image. Bar = 10 μm. Dot plot: *cis*-B7:CD28 N_{FRET} from n > 30 cells in three independent experiments. Mean ± SEM.

(C) Effects of SNX9 deficiency on *cis*-B7-induced synaptic enrichment of CD28 and PKCθ. Leftmost cartoons depict a $CD80^{-/-}CD86^{-/-}$ Raji cell contacting Jurkat cell with indicated

genotype. Further right are confocal images of immunostained CD28 and PKCθ acquired 30 min after Jurkat:Raji cell contact, with Raji cell denoted by a dash circle. Dot plots: synaptic enrichment indices of CD28 (magenta) and PKCθ (yellow), n > 16 conjugates in three independent experiments. Bar = 10 μm.

(D) Effects of SNX9 deficiency on *cis*-B7 induced IL-2 secretion. Western blot shows SNX9 and GAPDH expression in indicated Jurkat cells. Bar graph on the right summarizes IL-2 secretion from WT or *SNX9*$^{-/-}$ Jurkat cell with or without B7 transduced upon coculture with excess SEE-loaded *CD80*$^{-/-}$*CD86*$^{-/-}$ Raji cell in three independent experiments.

(E) 3D reconstructed Z-stack confocal images of SNX9, T cell membranes, and CD28 in the presence of *cis*-B7 upon TCR stimulation. Leftmost cartoons depict Jurkat cell with indicated genotype triggered by an anti-CD3ε (OKT3) containing SLB. On the right are 3D reconstruction images of mGFP-SNX9, R18-stained Jurkat cell membranes, and immunostained CD28(WT) or CD28(Y191F) acquired 30 min after Jurkat:SLB contact. Bar = 5 μm.

Unpaired two-tailed Student's t test for (B), One-way ANOVA for (C, D). **p < 0.01, ***p < 0.001, ****p < 0.0001.
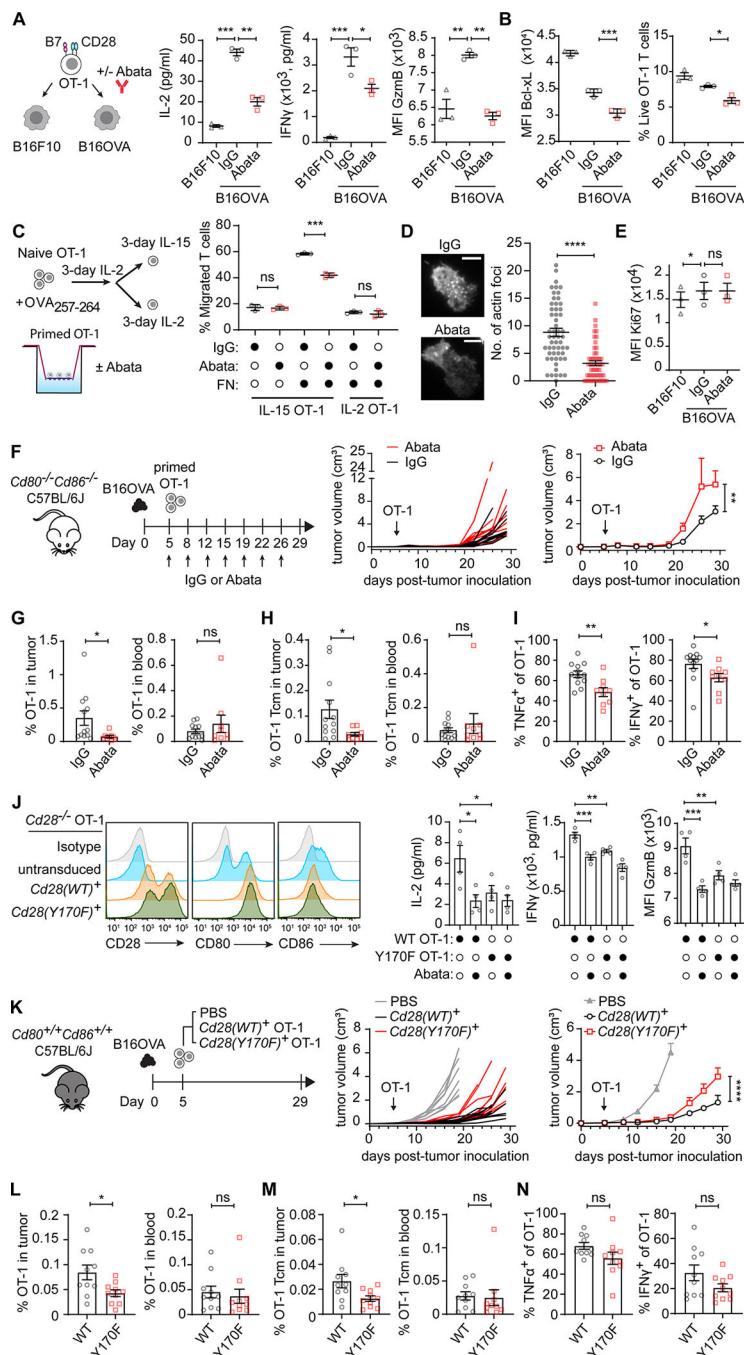
Figure 7. Disruption of *cis*-B7:CD28 interactions attenuates cytokine production, cytotoxicity, survival, migration and anti-tumor activity of CD8+ T cells.

(**A**) Dot plots summarizing IL-2, IFNγ, and GzmB productions from primed OT-1 cells after 24 h coculture with five-fold excess B7-negative B16F10 or B16OVA, in the presence of Abata or IgG control.

(**B**) Dot plots summarizing Bcl-xL expression and % live population of OT-1 cells after 72 h of OT-1:B16 cell co-culture depicted in A.

(C) OT-1 cell migration cross a FN-coated transwell in the presence of Abata or IgG control. OT-1 cells were pre-conditioned by IL-2 or IL-15 as depicted. Dot plots: % cells migrated to the bottom well in 4 h.

(D) Effects of *cis*-B7:CD28 interactions on actin foci formation. Left, TIRF images of actin foci in LifeAct-mCherry-transduced, IL-15 conditioned OT-1 cells seeded on an ICAM1-coated plate, in the presence of Abata or IgG control. Dot plot summarizes numbers of actin foci per cell from two independent experiments. n > 52 cells, bar = 5 μm.

(E) Effects of *cis*-B7:CD28 interactions on OT-1 cell proliferation. Same as (A) except measuring Ki67 expression.

(F) Effects of Abata on B16OVA tumor growth in $Cd80^{-/-}Cd86^{-/-}$ C57BL/6J mice adoptively transferred with OT-1 cells. Left, experimental scheme. Middle, tumor volume plotted against time for individual mice that received either Abata or IgG control. Right, mean tumor volume plotted against time for all mice in the indicated treatment group.

(G, H) Effects of Abata on total and Tcm OT-1 cells adoptively transferred to $CD80^{-/-}CD86^{-/-}$, B16OVA-bearing C57BL/6J mice, measured in tumor and blood at the end point.

(I) Effects of Abata on TNFα and IFNγ expression in tumor-infiltrating OT-1 cells. Data shown as mean ± SEM, n = 12 for IgG condition and n = 9 for Abata condition.

(J) Left, CD28, CD80 and CD86 expressions on $Cd28^{-/-}$ OT-1 cells reconstituted with *Cd28(WT)* or *Cd28(Y170F)*. Right, IL-2, IFNγ and GzmB production by indicated OT-1 cells upon 24 h coculture with OVA-loaded B16F10 cells. Data from 2 mice with 2 technical replicates each.

(K) B16OVA tumor growth in WT C57BL/6J mice transferred with *Cd28(WT)*[+] OT-1 cell or *Cd28(Y170F)*[+] OT-1 cell. Left, experimental scheme. Middle, tumor volume plotted against time for individual mice that received indicated OT-1 cell or PBS alone. Right, mean tumor volume plotted against time.

(L, M) Total and Tcm *Cd28(WT)*[+] OT-1 cells or *Cd28(Y170F)*[+] OT-1 cells in tumor and blood of OT-1 cell transferred mice at the end point.

(N) TNFα and IFNγ expression in tumor-infiltrating *Cd28(WT)*[+] OT-1 cell and *Cd28(Y170F)*[+] OT-1 cell. Data shown as mean ± SEM, n = 10 for each condition.

Unpaired two-tailed Student's t test for (C, D, G-I, L-N), One-way ANOVA for (A, B, E, J), Two-way ANOVA for (F, K). ns, p > 0.05, *p < 0.05, **p < 0.01, ***p < 0.001, ****p < 0.0001. See also Figures S5–S7.

Key resources table

REAGENT or RESOURCE	SOURCE	IDENTIFIER
Antibodies		
PE anti-human CD28 antibody	BioLegend	Cat # 302940 RRID: AB_2564147
Anti-human CD28 antibody	Bio X Cell	Cat # BE0291 RRID: AB_2687814
PE anti-human CD80 antibody	BioLegend	Cat # 305208 RRID: AB_314504
Allophycocyanin anti-human CD80 antibody	BioLegend	Cat # 305220 RRID:AB_2076147
Allophycocyanin anti-human CD86 antibody	BioLegend	Cat # 374207 RRID: AB_2721448
CF568 anti-mouse IgG antibody	Biotium	Cat # 20802 RRID: N/A
Anti-human CD3ε antibody	BioLegend	Cat # 317326 RRID: AB_11150592
Anti-SNX9 antibody	Proteintech	Cat # 15721-1-AP RRID: AB_2286415
Anti-GAPDH antibody	Proteintech	Cat # 10494-1-AP RRID: AB_2263076
AF647 anti-human CD28 antibody	BioLegend	Cat # 302953 RRID: AB_2721412
Anti-PKCθ antibody	Cell Signaling	Cat # 13643S RRID: AB_2798282
CF568 anti-rabbit IgG antibody	Biotium	Cat # 20801 RRID: N/A
Atezolizumab	Bio X Cell	Cat # SIM0009 RRID: AB_2894730
Biotin anti-human CD3ε antibody	BioLegend	Cat # 317320 RRID: AB_10916519
Anti-mouse CD3ε antibody	BioLegend	Cat # 100340 RRID: AB_11149115
Anti-mouse CD28 antibody	BioLegend	Cat # 102116 RRID: AB_11147170
TruStain FcX plus	BioLegend	Cat # 156604 RRID: AB_2783138
Allophycocyanin-Cy7 anti-mouse CD3ε antibody	BioLegend	Cat # 100330 RRID: AB_1877170
FITC anti-mouse CD4 antibody	BioLegend	Cat # 317408 RRID: AB_1877170
FITC anti-mouse CD4 antibody	BioLegend	Cat # 100510 RRID: AB_312713
PerCP-Cy5.5 anti-mouse CD8 antibody	BioLegend	Cat # 100734 RRID: AB_2075238
FITC anti-mouse CD8 antibody	BioLegend	Cat # 140404 RRID: AB_10643587
PE anti-mouse CD80 antibody	BioLegend	Cat # 104707 RRID: AB_313128
BV711 anti-mouse CD80 antibody	BioLegend	Cat # 104743 RRID: AB_2810338

REAGENT or RESOURCE	SOURCE	IDENTIFIER
Allophycocyanin anti-mouse CD86 antibody	BioLegend	Cat # 105011 RRID: AB_493343
PE-Cy7 anti-mouse CD28 antibody	BioLegend	Cat # 102126 RRID: AB_2617011
AF700 anti-human CD3ε antibody	BioLegend	Cat # 317339 RRID: AB_2563407
FITC anti-human CD4 antibody	BioLegend	Cat # 317408 RRID: AB_571951
PerCP-Cy5.5 anti-human CD8 antibody	BioLegend	Cat # 301031 RRID: AB_893426
PE-Cy7 anti-human CD28 antibody	BioLegend	Cat # 302926 RRID: AB_10644005
PE anti-human CD86 antibody	BioLegend	Cat # 374206 RRID: AB_2721633
BV711 human IFNγ antibody	BioLegend	Cat # 502539 RRID: AB_11218602
PE antti-mouse PD1 antibody	Biolegend	Cat # 109104 RRID: AB_313421
PE anti-mouse PDL1 antibody	Biolegend	Cat # 124308 RRID: AB_2073556
PE anti-GzmB antibody	BioLegend	Cat # 372207 RRID: AB_2687031
PE-Cy7 anti-mouse Ki67 antibody	BioLegend	Cat # 652425 RRID: AB_2632693
Anti-Bcl-xL antibody	Proteintech	Cat # 10783-1-AP RRID: AB_2064724
AF647 anti-rabbit IgG antibody	BioLegend	Cat # 406414 RRID: AB_2563202
BV785 anti-mouse CD45 antibody	BioLegend	Cat # 103149 RRID: AB_2564590
FITC anti-mouse CD8 antibody	Accurate Chemical	Cat # ACL168F RRID: N/A
BV610 anti-mouse CD8 antibody	Bio-Rad	Cat # MCA609SBV610 RRID: N/A
PE-Dazzle 594 anti-mouse CD62L antibody	BioLegend	Cat # 104448 RRID: AB_2566162
BV650 anti-mouse CD44 antibody	BioLegend	Cat # 103049 RRID: AB_2562600
BV711 anti-mouse IFNγ antibody	BioLegend	Cat # 505835 RRID: AB_11219588
AF488 anti-mouse TNFα antibody	BioLegend	Cat # 506315 RRID: AB_493329
Anti-mouse CD3ε antibody	Abcam	Cat # ab16669 RRID: AB_443425
Allophycocyanin anti-human CD69 antibody	Biolegend	Cat # 310909 RRID: AB_314844
HRP anti-rabbit IgG antibody	Cell IDX	Cat # 2RH-100 RRID: N/A
Biological samples		
Human white blood cells	San Diego Blood Bank	Cat # LRS-WBC's

REAGENT or RESOURCE	SOURCE	IDENTIFIER
Bacterial and virus strains		
Escherichia coli BL21 (DE3)	New England Biolabs	Cat # C2527I
Chemicals, peptides, and recombinant proteins		
Fetal bovine serum	Omega Scientific	Cat # FB-02
DMEM medium	Corning	Cat # 10017CV
RPMI 1640 medium	Corning	Cat # 10041CM
Sodium pyruvate	Corning	Cat # 25000CI
β-mercaptoethanol	Fisher Scientific	Cat # ICN19024283
Penicillin and Streptomycin	GE Healthcare	Cat # SV30010
Trypsin-EDTA (0.25%)	ThermoFisher Scientific	Cat # 25200114
Trypan blue	Sigma	Cat # T8154
HBSS	ThermoFisher Scientific	Cat # 14025134
PBS	ThermoFisher Scientific	Cart # 10010049
Everspark STORM buffer	Idylle	Cat # Everspark
100 nm Red Fluorescent Nanodiamond	Adámas Nanotechnologies	Cat # NDNV100nmHi2ml
Furimazine	Aobious	Cat # AOB36539
Janelia Fluor® 646, Maleimide	Tocris Bioscience	Cat # 6590
Alexa Fluor® 647 Streptavidin	Jackson ImmunoResearch	Cat # 016-600-084
Poly-D-Lysine	Sigma-Aldrich	Cat # P6407
Polyethylenimine	Fisher Scientific	Cat # NC1014320
CLIP-Surface Dy547	New England Biolabs	Cat # S9233S
SNAP-Surface Alexa Fluor 647	New England Biolabs	Cat # S9136S
Paraformaldehyde	Fisher Scientific,	Cat # 50980494
Glutaraldehyde	Electron Microscopy Sciences	Cat # 16020
Sodium cacodylate	Electron Microscopy Sciences	Cat # 12300
Triton X-100	Fisher BioReagents,	Cat # BP151500
LgBiT-SpyCatcher	This study	N/A
SpyCatcher-AVI	This study	N/A
AP-SpyCatcher	This study	N/A
EX-NbALFA	This study	N/A
BirA	X. Xu, et al., 2021	N/A
HisTrap HP column	GE Healthcare	Cat # 17524802
Glutathione Agarose Beads	MCLAB	Cat # GAB-300
Superdex 75 Increase 10/300 GL column	GE Healthcare	Cat # 29148721
Superdex 200 Increase 10/300 GL column	GE Healthcare	Cat # 28990944
Zeba Spin Desalting Columns	ThermoFisher Scientific	Cat # P187769
Bovine serum albumin	ThermoFisher Scientific	Cat # 23209
SEE	Toxin Technology	Cat # ET404
SEB	Toxin Technology	Cat # BT202

REAGENT or RESOURCE	SOURCE	IDENTIFIER
ViaFluor 405 SE	Biotium	Cat # 30068
Saponin	MilliporeSigma	Cat # 558255
Abatacept	Ira Mellman (Genentech)	N/A
Human IgG1 Fc	Bio X Cell	Cat # BE0096
Rapamycin	Fisher BioReagents	Cat # 501126903
Hemin	Sigma Aldrich	Cat # H9039
DAB	TCI Chemicals	Cat # D0077
1-palmitoyl-2-oleoyl-sn-glycero-3-phosphocholine (POPC)	Avanti Polar Lipids	Cat # 850457C
1,2-dioleoyl-sn-glycero-3-[(N-(5-amino-1-carboxypentyl) iminodiacetic acid) succinyl] (nickel salt, DGS-NTA-Ni)	Avanti Polar Lipids	Cat # 790404C
1,2-Dipalmitoyl-sn-glycero-3-phosphoethanolamine-N-(biotinyl) (sodium salt, Biotin-DPPE)	Avanti Polar Lipids	Cat#: 870285P
1,2-Dioleoyl-sn-glycero-3-phosphoethanolamine-N-[methoxy(polyethylene glycol)-5000] ammonium salt (PEG5000-PE)	Avanti Polar Lipids	Cat#: 880230C
Streptavidin	ThermoFisher Scientific	Cat # S888
Human ICAM1	Sino Biological	Cat # 10346-H08H
Human IL-2	PeproTech	Cat # 200-02
Human IL-15	PeproTech	Cat # 200-15
Mouse IFNγ	Biolegend	Cat # 575302
OVA$_{257-264}$	Anaspec	Cat # AS-60193-1
Zombie Violet	BioLegend	Cat # 423113
Zombie Aqua	BioLegend	Cat # 423102
Fibronectin	Corning	Cat # 354008
Mouse ICAM1	Sino Biological	Cat # 50440-M08H
BV421 OVA$_{257-264}$ H-2K^b tetramer	NIH Tetramer Core Facility	N/A
Tyramide-488 Reagent	ThermoFisher Scientific	Cat # B40953
Octadecyl Rhodamine B Chloride	Biotium	Cat # 60033
Brefeldin A	Biolegend	Cat # 420601
Collagenase	Worthington Biochemical	Cat # LS004197
Soybean trypsin inhibitor	Worthington Biochemical	Cat # LS003587
Critical commercial assays		
Human IL-2 ELISA MAX™	BioLegend	Cat # 431804
Mouse IL-2 ELISA MAX™	BioLegend	Cat # 431001
Mouse IFNγ ELISA MAX™	BioLegend	Cat # 430801
PCR Mycoplasma Detection Kit	Applied Biological Materials Inc	Cat # G238
Mouse CD3 T cell isolation kit	BioLegend	Cat # 480031
mouse CD8 naïve T cell isolation kit	BioLegend	Cat # 480044
Experimental models: Cell lines		
HEK 293T cells	Ronald Vale (University of California San Francisco)	RRID: CVCL_0063

REAGENT or RESOURCE	SOURCE	IDENTIFIER
Phoenix-ECO cells	Ronald Vale (University of California San Francisco)	RRID: CVCL_H717
Platinum E cells	Li-Fan Lu (University of California San Diego)	RRID: CVCL_B488
Jurkat E6.1 T cells	Arthur Weiss (University of California San Francisco)	RRID: CVCL_0065
Raji B cells	Ronald Vale	RRID: CVCL_0511
B16F10	ATCC	Cat # CRL-6475, RRID: CVCL_0159
B16OVA	Ananda Goldrath	N/A
See Table S1 for the list of cell lines	This study	N/A
Experimental models: Organisms/strains		
C57BL/6-Tg (TcraTcrb) 1100Mjb/J (OT-1)	Jackson Laboratory	RRID: IMSR_JAX:003831
B6.129S4-Cd80tm1Shr Cd86tm2Shr/J ($Cd80^{-/-}Cd86^{-/-}$)	Jackson Laboratory	RRID: IMSR_JAX:003610
C57BL/6J	Jackson Laboratory	RRID: IMSR_JAX:000664
B6.129S2-Cd28tm1Mak/J ($Cd28^{-/-}$)	Jackson Laboratory	RRID: IMSR_JAX:002666
$Cd28^{-/-}$ OT-1	This study	N/A
Oligonucleotides		
CD28 sgRNAs: 5'-GCTTGTAGCGTACGACAATG-3' and 5'-GTCCTTTGTGAAGGGATGCC-3'	This study	N/A
SNX9 sgRNAs: 5'-AATGAACTGACGGTTAATGA-3' and 5'-GAAACATCAAAGGAGAACGA-3'	Ecker, et al., 2022	N/A
Recombinant DNA		
See Table S2 for the list of recombinant DNAs	This study	N/A
Software and algorithms		
ImageJ	NIH	https://imagej.nih.gov/ij/
Micro-Manager	Open Imaging, Inc.	https://micro-manager.org/
AccPbFRET	(Roszik et al., 2008)	http://biophys.med.unideb.hu/accpbfret/
GraphPad Prism	GraphPad Software Inc.	https://www.graphpad.com/scientific-software/prism/
FlowJo	FlowJo, LLC	https://www.flowjo.com/
ThunderSTORM	(Ovesný et al., 2014)	https://zitmen.github.io/thunderstorm/
Coloc-Tesseler software	(Levet et al., 2019)	http://www.iins.u-bordeaux.fr/team-sibarita-Coloc-Tesseler
PyMOL	Schrödinger, Inc	https://pymol.org/2/ RRID:SCR_000305